HHS Public Access

Author manuscript

Cell Rep. Author manuscript; available in PMC 2022 January 03.

Published in final edited form as:

Cell Rep. 2020 March 24; 30(12): 4027–4040.e7. doi:10.1016/j.celrep.2020.03.006.

An mRNA-mRNA Interaction Couples Expression of a Virulence Factor and Its Chaperone in *Listeria monocytogenes*

Dmitriy Ignatov[1,2,3,4,9,*], **Karolis Vaitkevicius**[1,2,3], **Sylvain Durand**[5], **Laty Cahoon**[6], **Stefanie S. Sandberg**[1,2,3], **Xijia Liu**[7], **Birgitte H. Kallipolitis**[8], **Patrik Rydén**[7], **Nancy Freitag**[6], **Ciarán Condon**[5], **Jörgen Johansson**[1,2,3,10,*]

[1]Department of Molecular Biology, Umeå University, SE-901 87 Umeå, Sweden

[2]Umeå Centre for Microbial Research, Umeå University, Umeå, Sweden

[3]Laboratory for Molecular Infection Medicine Sweden (MIMS), Umeå University, Umeå, Sweden

[4]Laboratory for Genomic Engineering, Moscow Institute of Physics and Technology, Dolgoprudniy, Russia

[5]UMR8261 CNRS Universitéde Paris, Institut de Biologie Physico-Chimique, Paris, France

[6]Department of Microbiology and Immunology, University of Illinois at Chicago, Chicago, IL 60612, USA

[7]Department of Mathematics and Mathematical Statistics, Umeå University, Umeå, Sweden

[8]Department of Biochemistry and Molecular Biology, University of Southern Denmark, Odense, Denmark

[9]Present address: Max Planck Unit for the Science of Pathogens, Chariteplatz 1, 10117 Berlin, Germany

[10]Lead Contact

SUMMARY

Bacterial pathogens often employ RNA regulatory elements located in the 5′ untranslated regions (UTRs) to control gene expression. Using a comparative structural analysis, we examine the structure of 5′ UTRs at a global scale in the pathogenic bacterium *Listeria monocytogenes* under different conditions. In addition to discovering an RNA thermoswitch and detecting simultaneous interaction of ribosomes and small RNAs with mRNA, we identify structural changes in the 5′ UTR of an mRNA encoding the post-translocation chaperone PrsA2 during infection conditions.

*Correspondence: dima.ignatov@gmail.com (D.I.), jorgen.johansson@umu.se (J.J.).

AUTHOR CONTRIBUTIONS

Conceptualization, D.I., S.D., C.C., and J.J.; Methodology, D.I., P.R., and J.J.; Software, D.I.; Validation, D.I.; Formal Analysis, D.I., S.D., and P.R.; Investigation, D.I., K.V., S.D., L.C., S.S.S., and X.L.; Resources, J.J., C.C., B.H.K., and N.F.; Writing – Original Draft, D.I. and J.J.; Writing – Review and Editing, D.I., K.V., S.D., S.S.S., L.C., B.H.K., N.F., P.R., C.C., and J.J.; Visualization, D.I. and J.J.; Project Administration, J.J.; Funding Acquisition, S.D., C.C., and J.J.

DECLARATION OF INTERESTS

The authors declare no competing interests.

SUPPLEMENTAL INFORMATION

Supplemental Information can be found online at https://doi.org/10.1016/j.celrep.2020.03.006.

We demonstrate that the 5′ UTR of the *prsA2* mRNA base pairs with the 3′ UTR of the full-length *hly* mRNA encoding listeriolysin O, thus preventing RNase J1-mediated degradation of the *prsA2* transcript. Mutants lacking the *hly-prsA2* interaction exhibit reduced virulence properties. This work highlights an additional level of RNA regulation, where the mRNA encoding a chaperone is stabilized by the mRNA encoding its substrate.

In Brief

By using a comparative structural analysis method targeting 5′ untranslated regions, Ignatov et al. identify different RNA-based regulatory mechanisms such as an RNA thermoswitch, a small RNA (sRNA)-mRNA interaction, and strikingly, an mRNA-mRNA interaction.

Graphical Abstract

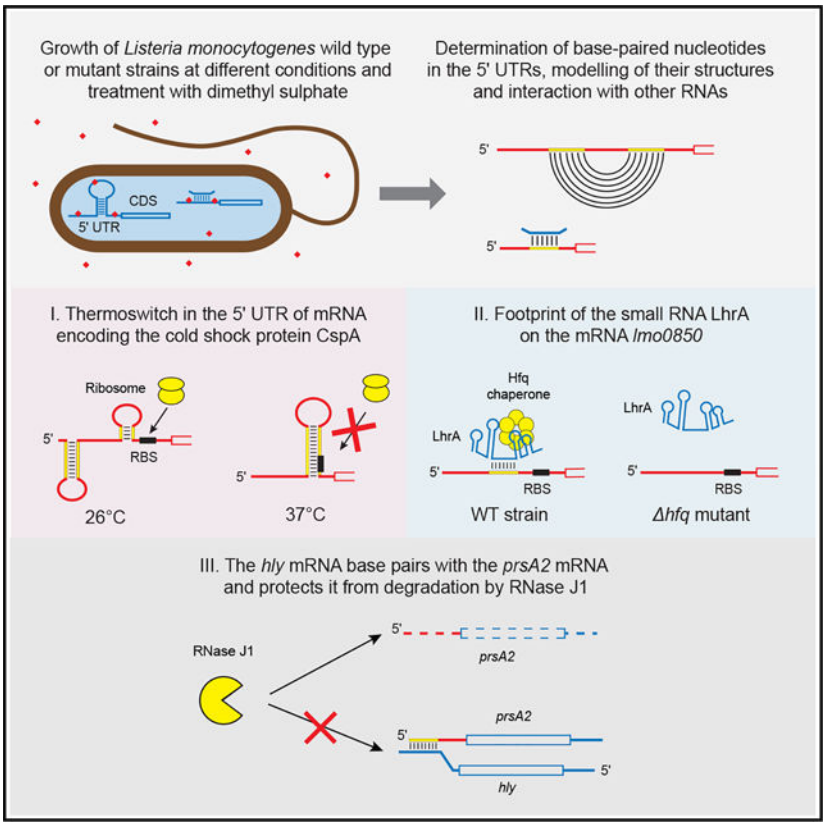

INTRODUCTION

Within the cytosol of living cells, RNA molecules fold into complex structures that are important for their functions (Miao and Westhof, 2017). In bacteria, regulatory RNAs control gene expression in response to changes in physical and chemical parameters, and binding of proteins, metabolites, or other RNA molecules, and their mechanism of action is often based on alteration of RNA structure (Meyer, 2017).

Small RNAs (sRNAs) represent a widespread class of regulators in bacteria and have long served as a paradigm for *trans*-encoded RNA regulators. However, recent data suggest that protein-coding transcripts can also base pair *in trans* and perform regulation. Genomes of different bacterial species encode dual-function sRNAs, which not only encode peptides or short proteins but also base pair with other RNAs (Raina et al., 2018). Moreover, even canonical mRNAs with lengths exceeding 500 nt can engage in regulatory base-pairing interactions. As an example, intramolecular base-pairing between the 5′ and 3′ untranslated regions (UTRs) regulates expression of the *icaR* mRNA in *Staphylococcus aureus* (Ruiz de los Mozos et al., 2013). A similar mechanism regulates expression of toxin mRNAs in some type I toxin-antitoxin systems (Masachis and Darfeuille, 2018). Moreover, a canonical mRNA *irvA* in *Streptococcus mutans* has been shown to base pair with another mRNA, *gbpC*, and protect it from degradation (Liu et al., 2015). These discoveries suggest that the network of regulatory base-pairing interactions in bacteria can be more complex than previously anticipated.

Pathogenic bacteria employ regulatory RNAs to adapt to living conditions inside the host and orchestrate the development of their virulence programs (Chakravarty and Massé, 2019). The facultative pathogen *Listeria monocytogenes* has served as a model for extensive research on RNA regulation (Lebreton and Cossart, 2017). Studies of several *L. monocytogenes* sRNAs facilitated the identification of genes that they regulate in the context of pathogenesis (Dos Santos et al., 2018; Nielsen et al., 2011, 2011; Quereda et al., 2014; Ross et al., 2019; Sievers et al., 2014, 2015). Another example of RNA regulation is an RNA thermometer controlling translation of the *prfA* mRNA, encoding the master regulator of *L. monocytogenes* virulence. During infection, PrfA induces expression of the major virulence genes (de las Heras et al., 2011). The RNA thermometer is located in the 5′ UTR of *prfA* mRNA and inhibits translation initiation at 30°C, but not 37°C, the latter temperature encountered when the pathogen enters the host (Johansson et al., 2002). The *prfA* 5′ UTR is also able to form base-pairing interactions with processed SAM riboswitches, which adds further complexity to RNA regulatory networks in *L. monocytogenes* (Loh et al., 2009).

The development of high-throughput RNA structure probing approaches has made it possible to profile the secondary structure of RNA molecules inside the cell on a transcriptome-wide scale (Mitchell et al., 2019; Strobel et al., 2018). These approaches were employed in bacteria to study how RNA structure affects translation (Burkhardt et al., 2017; Mustoe et al., 2018), discover G-quadruplexes (Guo and Bartel, 2016), and monitor RNA folding states during the response to the cold shock (Zhang et al., 2018). The action of regulatory RNA elements can be traced by the alterations of their structures. Comparison of structures of selected RNAs or the whole transcriptome has previously been used to discover novel regulatory elements in bacteria and eukaryotes (McGinnis et al., 2015; Mizrahi et al., 2018; Righetti et al., 2016).

The 5′ UTRs of bacterial mRNAs often serve as an important hub for RNA regulation, affecting the level of translation initiation or stability of transcripts (Oliva et al., 2015; Waters and Storz, 2009). To identify new RNA-based regulatory mechanisms in *L. monocytogenes*, we performed comparative analysis of 5′ UTR structures using an approach based on dimethyl sulfate (DMS) mutational profiling with sequencing (DMS-MaPseq)

method (Zubradt et al., 2017). Our work revealed an RNA thermoswitch regulating expression of the cold shock protein CspA. We also identified a case of simultaneous binding of a sRNA and the ribosome competing for the same transcript. Remarkably, our data also provided evidence for an mRNA-mRNA interaction in virulence-inducing conditions. The 5′ UTR of the *prsA2* mRNA interacts with the 3′ UTR of *hly*, encoding listeriolysin O (LLO), an important virulence factor in *L. monocytogenes*. The PrsA2 chaperone is necessary for the folding of LLO and other virulence factors during infection. The *hly-prsA2* interaction protected the *prsA2* transcript from degradation by RNase J1, thus allowing increased PrsA2 expression. An absence of the mRNA-mRNA interaction decreased cell-to-cell spread and reduced bacterial virulence in infected mice. Our results suggest an additional level of *L. monocytogenes* virulence regulation beyond the master virulence regulator PrfA, where an mRNA encoding a chaperone can directly bind and stabilize the mRNA encoding its substrate.

RESULTS

Profiling the RNA Structure of 5′ UTRs in *Listeria monocytogenes*

We adapted a DMS-MaPseq protocol (Zubradt et al., 2017) to focus on the dynamics of 5′ UTR structures in the bacterial pathogen *L. monocytogenes* (Figure 1). Most bacterial regulatory RNA domains so far identified are located in the 5′ UTRs of mRNA molecules or in sRNAs. Our protocol (FUSE for 5′ UTR structure elucidation) selectively enriches for 5′ UTRs and sRNAs. In brief, DMS selectively methylates the Watson-Crick surfaces of unpaired adenine or cytosine nucleotides, but not when these bases are paired (intramolecularly or intermolecularly) or bound to proteins. After ligation of 5′ adapters, the RNA is fragmented, and the 3′ adapters are ligated. Using a reverse transcriptase (TGIRTIII) that incorporates a random base upon encountering a methylated adenine or cytosine, cDNA is produced. Base substitutions in the sequences indicate unpaired adenines or cytosines and using dedicated algorithms, the nucleotides changing their base-pairing interactions can be identified. Bacterial cells with different genetic backgrounds (Table S1) were grown at different conditions (Table S2) and treated with DMS during growth (*in vivo* samples). Alternatively, RNA isolated from cells was refolded, and DMS modification was performed (*in vitro* samples). After DMS treatment, DMS values were calculated for each adenine and cytosine in the 5′ UTRs and sRNAs. The DMS value represents a normalized measure of DMS modification and was used to predict RNA secondary structures, and the FUSE protocol increases the sequencing coverage of 5′ UTRs (Figure S1; Table S3).

Because no crystal structures have been solved for *L. monocytogenes* regulatory RNAs, we predicted the secondary structure of evolutionarily conserved 4.5S RNA using its structure in *B. subtilis* and *E. coli* as a blueprint (Nakamura et al., 1992). To verify the reliability of the method, we studied how well the calculated DMS values fit the predicted structure. In general, all base-paired nucleotides in 4.5S RNA had DMS values lower than 1, whereas most of the unpaired nucleotides had DMS values higher than 1 (Figures S2A and S2B). Some of the nucleotides not predicted to base pair also showed low DMS values, suggesting that these nucleotides can participate in tertiary interactions or be protected from DMS modification by other mechanisms. Indeed, during the analysis of 4.5S RNA structure, we

noticed that several nucleotides in the evolutionarily conserved domain IV had significantly lower DMS values *in vivo* compared with *in vitro* (Figures 2A and S2C). The most dramatic changes were observed for nucleotides A151 and A159. In *Escherichia coli*, nucleotides in these positions directly interact with the M domain of the Ffh protein (Figure 2B; Batey et al., 2000, 2001).

Second, we used the *prfA* thermosensor as a reference to compare our FUSE data with the previously identified secondary structure of the *prfA* RNA thermoswitch (Johansson et al., 2002). In most samples, the expression of the monocistronic *prfA* mRNA was too low to probe its DMS reactivity. Only in FUSE libraries where DMS treatment was performed *in vitro* and in the *prfA** bacterial strain with PrfA regulator constantly activated did we obtain enough coverage to profile the structure of *prfA* 5′ UTR. The structure of the thermoswitch in the *in vitro* and *in vivo* samples agree well with each other and with the published structure (Figure S2D; Johansson et al., 2002). To detect changes associated with *prfA* thermoswitch melting, we employed targeted DMS-MaPseq of the *prfA* 5′ UTR region in bacteria growing at 26°C and 37°C. The structural differences identified in the thermoswitch between two temperatures were limited. However, we identified a higher DMS reactivity of some critical bases, such as C98, which needs to be base paired to prevent PrfA expression and virulence gene expression at 30°C (Figure S2E; Johansson et al., 2002). In conclusion, we consider FUSE to be a reliable approach to determine RNA secondary structures.

Shine-Dalgarno Sequences Are Occupied by Ribosomes *In Vivo*

We compared the average DMS values of 5′ UTRs *in vitro* and inside the cell. Globally, the nucleotides in positions 10–15 upstream of the start codon had considerably lower DMS values *in vivo* compared with *in vitro* (Figure 2C). This region overlaps with the distribution of Shine-Dalgarno (SD) sequences in *L. monocytogenes* mRNAs. A previous study performed *in vitro* on a selected mRNA demonstrated that binding of the 30S ribosome subunit confers DMS protection for the nucleotides of the SD sequence (Hüttenhofer and Noller, 1994). Interestingly, the DMS values of SD sequences in samples prepared *in vitro* (without ribosomes) showed the opposite trend and were slightly higher compared with flanking regions (Figure 2C). This suggests that SD sequences generally do not base pair, thereby facilitating the interaction with 30S ribosome subunits, as has been suggested previously (Righetti et al., 2016). We suggest that the low DMS reactivity of the SD sequences we observed *in vivo* on a global level can be explained by the interaction with ribosomes, through base-pairing interactions between the SD sequences of mRNAs and the anti-SD sequences of 16S rRNA. Hence FUSE can predict structural changes that might indicate the binding of other factors.

Comparison of 5′ UTR Structures at Different Temperatures Uncovers a Thermoswitch Controlling Expression of a Cold Shock Protein

A comparison of DMS values in *L. monocytogenes* cells grown at different temperatures detected significant structural changes in the 5′ UTR of the *cspA* (*lmo1364*) mRNA (Table S4). This gene encodes a cold shock protein that plays an important role in the adaptation of *L. monocytogenes* to low temperatures (Schmid et al., 2009). Using DMS values as guides for structure modeling, we reconstructed two alternative conformations for this 5′

UTR: at 26°C, the structure adopted an “open” conformation, where the SD sequence was available for ribosome binding, whereas at 37°C, the 5′ UTR rearranged to a “closed” conformation with the SD sequence hidden in an RNA hairpin (Figures 3A and S3A). This was especially evident after a transient shift from 26°C to 37°C. To study the putative effect of the rearrangement on translation, we introduced mutations in the *cspA* 5′ UTR structure that destabilized either the open or closed conformation (Figures 3A and S3B) and created translational fusions of the wild-type (WT) and mutant 5′ UTRs to the β-galactosidase gene. As controls, translational fusions of three short 5′ UTRs that do not form stable secondary structures were constructed. The expression of the translational fusions was measured in *Escherichia coli* at different temperatures. Expression of the control fusions was higher at 37°C than at 26°C, whereas the WT *cspA* 5′ UTR reduced β-galactosidase expression at 37°C (Figure 3B). Mutation M1 destabilized the open conformation and inhibited expression at both 26°C and 37°C, whereas introduction of mutation M2 complementary to M1 restored the WT expression pattern. Mutation M3 destabilized the closed conformation and abolished inhibition at 37°C, causing high expression at both temperatures, whereas its complementary mutation M4 restored the expression pattern observed in the WT. To examine whether other cellular factors were required for the structural rearrangement of the *cspA* 5′ UTR, we synthesized the WT thermoswitch and its mutated isoforms *in vitro* and denatured and refolded them at different temperatures. The folding into open or closed conformation was identifiable by their different electrophoretic mobilities in non-denaturing polyacrylamide gels. The WT thermoswitch migrated more rapidly when refolded at 26°C than at 37°C, suggesting a higher electrophoretic mobility of the open conformation, whereas the M1 mutant RNA, which is locked in the closed conformation, demonstrated low mobility at both temperatures (Figure 3C). In contrast, the electrophoretic mobility of the M3 mutant RNA, which is locked in the open conformation, was high at both temperatures, whereas the compensatory mutations (M1+M2 and M3+M4) restored the migration to the pattern observed for the WT *cspA* 5′ UTR (Figure 3C). Refolding of the WT *cspA* 5′ UTR at different temperatures ranging from 26°C to 34°C demonstrated that the transition from the open to closed conformation occurs at approximately 30°C (Figure 3D). These data were further verified by performing DMS-MaPseq of *in-vitro*-synthesized *cspA* 5′ UTR that was denatured and refolded at 26°C or 37°C. The structure of the *cspA* 5′ UTR refolded at 26°C showed a more open conformation, whereas the *cspA* 5′ UTR refolded at 37°C adopted a closed conformation (Figure S3C). Together, our data show that the *cspA* 5′ UTR in *L. monocytogenes* represents a bona fide RNA thermoswitch. The structure corresponding to the open conformation of the thermoswitch is conserved in all *Listeriaceae* and in some other species in the orders Bacillales and Lactobacillales (Figure S3D). However, it is structurally different from the *cspA* thermoswitch in *Escherichia coli* (Figure S3E; Giuliodori et al., 2010; Zhang et al., 2018).

Simultaneous Binding of Ribosomes and sRNAs Can Be Defined by FUSE

Many bacterial species require Hfq to establish a functional interaction between sRNAs and their target mRNAs (Updegrove et al., 2016). However, in Firmicutes and *L. monocytogenes* in particular, the role of Hfq seems to be limited (Nielsen et al., 2010). We therefore studied how deletion of the RNA chaperone Hfq affects the structure of 5′ UTRs globally. Indeed, the *Δhfq* strain showed very modest changes in the 5′ UTR structurome in comparison with

the WT (Table S4). The strongest changes were observed in the sRNA LhrA (Figure S4) and the 5′ UTR of the *lmo0850* mRNA (Figure 3E). It has previously been shown that LhrA interacts with the *lmo0850* mRNA in a Hfq-dependent manner both *in vivo* and *in vitro* (Nielsen et al., 2010). In agreement with this, we observed that the nucleotides of the *lmo0850* mRNA known to form base-pairing interactions with LhrA had significantly higher DMS values in the *Δhfq* strain, supporting the fact that the interaction is abolished in the absence of the chaperone (Figures 3E and 3F). On the contrary, the DMS values of nucleotides in the SD sequence of *lmo0850* were decreased in the *Δhfq* strain, correlating with stronger ribosome binding when LhrA is not bound. These data agree fully with the previous study showing that the LhrA-*lmo0850* interaction inhibits formation of a translation initiation complex and represses translation (Nielsen et al., 2010). A similar profile was observed in the *Δhfq* mutant and in the *LhrA-mut* strain, bearing substitutions in the LhrA sequence at its interaction site with *lmo0850* (i.e., increased reactivity at the LhrA interaction site and decreased reactivity at the SD region). Hence, at the single-nucleotide resolution, we were able to simultaneously follow the binding of the ribosome and LhrA sRNA to the *lmo0850* transcript *in vivo* (Figure 3F).

The Activation of the *L. monocytogenes* Virulence Program Induces DMS Protection of the 5′ UTR of the *prsA2* mRNA

L. monocytogenes is a facultative pathogen that can switch between the lifestyles of an environmental bacterium and a dangerous intracellular pathogen. The major player in this transition is the transcriptional regulator PrfA (de las Heras et al., 2011). Upon entry of the bacterium into the mammalian cell, PrfA recognizes glutathione as a host signal and directly activates expression of the most important virulence genes (Reniere et al., 2015). We hypothesized that an induction of the virulence program upon PrfA activation might have an influence on the 5′ UTR structures of the virulence-associated mRNAs, especially because *L. monocytogenes* appear to harbor many such transcripts with long 5′ UTRs (Loh et al., 2006). Also, several genes are positively regulated by PrfA but do not have an obvious PrfA binding site, suggesting they are indirectly regulated by PrfA (Milohanic et al., 2003). To examine this, we compared the 5′ UTR structures in the WT and *prfA** strains of *L. monocytogenes*. The *prfA** strain carries a G145S substitution in the PrfA protein, which makes the regulator constitutively active and permits high expression of virulence genes even during growth in broth culture (Ripio et al., 1997). Our comparison identified a group of nucleotides in the 5′ UTR of *prsA2* (*lmo2219*) mRNA that were protected from DMS in the *prfA** strain compared with WT (Figure 4A; Table S4). PrsA2 is predicted to function as a peptidyl-prolyl isomerase chaperone that assists in the folding of secreted proteins at the interface between the bacterial membrane and cell wall. In particular, PrsA2 promotes secretion and stability of the most significant virulence factor, LLO (Alonzo et al., 2009; Zemansky et al., 2009). Importantly, the absence of PrsA2 severely attenuates *L. monocytogenes* infectivity by up to 5 orders of magnitude (Alonzo and Freitag, 2010; Alonzo et al., 2009, 2011; Cahoon and Freitag, 2015; Cahoon et al., 2016; Port and Freitag, 2007; Zemansky et al., 2009). Although expression of the *prsA2* gene was shown to be dependent on PrfA activation (Figure S5A; Milohanic et al., 2003), the deletion of the PrfA binding site from the *prsA2* promoter did not eliminate *prsA2* expression (Zemansky et al., 2009).

The 3′ UTR of *hly* Directly Interacts with the 5′ End of *prsA2*

One possible reason why the nucleotides in the *prsA2* 5′ UTR showed an altered DMS protection may be due to RNA-RNA or RNA-protein interactions. Previously, it has been shown that the *trans*-acting sRNA RoxS is able to bind and prevent degradation of the *yflS* mRNA, by binding at its extreme 5′ end (Durand et al., 2017). With this in mind, we performed a whole-genome search for sequences complementary to the identified DMS footprint using the CopraRNA software (Table S5; Wright et al., 2014). Unexpectedly, the best match was in the 3′ UTR of the *hly* (*lmo0202*) mRNA, encoding LLO. Expression of the *hly* gene is directly regulated by PrfA and is much higher in the *prfA** strain than in the WT strain (Figures S5A and S5B; Ripio et al., 1997). Our data thus suggested a base-pairing interaction between the 5′ UTR of *prsA2*, encoding the chaperone, and the 3′ UTR of *hly* mRNA, encoding its substrate. To validate this interaction, we introduced complementary base substitutions in the chromosome corresponding to the proposed site of interaction between the *prsA2* 5′ UTR (M1) and the *hly* 3′ UTR (M2) (Figure 4A). These mutations disrupt the GC-rich motif located in the center of the putative *hly-prsA2* interaction site and when introduced alone should significantly diminish the mRNA-mRNA interaction. However, the simultaneous introduction of the complementary M1 and M2 mutations (strain M1+M2) should restore the base-pairing interaction between *hly* and *prsA2*. Despite several attempts, the strain simultaneously carrying both M1 and M2 mutations could not be created in the *prfA** strain background. Instead, we introduced chromosomal mutations in WT *L. monocytogenes* and induced virulence factor expression by growing bacteria in a special medium containing glucose-1-phosphate and a polymeric non-polar adsorbent (Figure S5B; Ermolaeva et al., 2004). The M1 and M2 mutant strains had significantly lower *prsA2* mRNA levels and protein levels compared with the WT strain (Figures 4B and 4C). In contrast, the M1+M2 mutant had *prsA2* and PrsA2 levels almost as high as the WT. Our results thus suggest that the 3′ UTR of the *hly* transcript is able to directly bind 5′ UTR of the *prsA2* transcript. Importantly, none of these mutations significantly affected the levels of the *hly* mRNA or LLO protein expression. An increased appearance of truncated LLO was observed in the M1 and M2 mutant strains, when the level of PrsA2 was reduced, as has been shown previously (Figure 4C, arrow; Alonzo et al., 2009). Whether this is due to an increased proteolysis and/or synthesis of shorter peptide due to partial degradation of the *prsA2* transcript is unknown.

The DMS profile of the *prsA2* (*lmo2219*) 5′ UTR in the *Δhfq* strain did not show any difference with the WT *L. monocytogenes* (Table S4), suggesting that the interaction between *hly* and *prsA2* mRNAs does not require the Hfq chaperone.

The Regulatory Region in the 3′ UTR Is Part of the Full-Length *hly* Transcript

The 3′ UTR regions of bacterial mRNAs can serve as reservoirs for sRNAs and are produced either by transcription from internal promoters or by mRNA processing (Miyakoshi et al., 2015). We therefore examined whether the regulatory region in the *hly* 3′ UTR was present as a short form or as a part of the full-length *hly* transcript. The northern blot results showed that the *hly* 3′ UTR was exclusively detected as part of the full-length *hly* transcript (Figures 4D and S5C). This is in line with previous studies where analysis of *L. monocytogenes* transcriptomes did not detect any short transcripts generated from the 3′

end portion of the *hly* mRNA (Mraheil et al., 2011; Toledo-Arana et al., 2009). In contrast, we readily detected the short RNA Rli51, originating from the 5′ UTR of the *mpl* mRNA (Toledo-Arana et al., 2009). Hence our data strongly indicate that the full-length *hly* mRNA acts *in trans* by a direct interaction with the *prsA2* mRNA.

hly Protects *prsA2* mRNA from RNaseJ1-Mediated Degradation

In contrast with the LhrA-*lmo0850* interaction (Figure 3E), we did not observe increased DMS protection of the *prsA2* SD sequence upon interaction with *hly*, indicating that the *hly-prsA2* interaction does not affect ribosome binding (Figure 4A). Furthermore, abolition of the interaction between the *prsA2* and *hly* mRNAs decreased the quantities of both *prsA2* mRNA and PrsA2 protein equally, suggesting that the *hly-prsA2* interaction might instead affect the stability of the *prsA2* mRNA (Figures 4B and 4C). To examine this, we measured *prsA2* mRNA stability following addition of rifampicin to prevent new transcription initiation. The half-life of *prsA2* mRNA was reduced in the M1 and M2 mutant strains lacking a functional *hly-prsA2* interaction (Figures 5A and S5D). In agreement with the expression data, the half-life of the *prsA2* transcript was increased in the M1+M2 double-mutant strain, in which the *hly-prsA2* interaction was restored. Unexpectedly, we observed a similar pattern of *prsA2* transcript stability in the strains also at non-inducing conditions (Figure 5A), suggesting that *hly* also stabilizes *prsA2* under non-inducing conditions, despite being expressed at much lower levels.

Our data suggest that the *hly* mRNA interacts with the extreme 5′ end of the *prsA2* mRNA (Figure 4A). In *Bacillus subtilis*, RoxS binding to the extreme 5′ end of the *yflS* mRNA protects it from the 5′–3′ exoribonuclease activity of RNase J1 (Durand et al., 2017). *L. monocytogenes* is very similar to *B. subtilis* with respect to the set of RNases that these organisms use for RNA degradation (Durand et al., 2015). We therefore examined whether *hly* binding could protect the *prsA2* mRNA from degradation by RNase J1. RNA fragments representing the 5′ UTR of the WT *prsA2* and the M1 mutant derivative were transcribed *in vitro*. The RNAs contained a ^{32}P-labeled 5′-monophosphate group to mimic removal of the 5′-triphosphate group by RNA pyrophosphohydrolase activity *in vivo*, allowing access to RNase J1. RNase J1-mediated 5′–3′ exoribonuclease activity caused the liberation of the first nucleotide, ^{32}P-labeled GMP, and this was used as a measure of RNase J1 activity (Durand et al., 2017). The WT *prsA2* and *prsA2-M1* RNAs were subjected to degradation by RNase J1 alone, or in the presence of the *hly* mRNA with a WT 3′ UTR or *hly-M2* mutant mRNA (124 nt) (Figures 5B and 5C). The accumulation of free GMP indicated rapid degradation of both *prsA2* and *prsA2-M1* transcripts by RNase J1 in the absence of the *hly* mRNA (Figures 5B and 5D). The degradation of the WT *prsA2* was significantly inhibited by the addition of *hly*, whereas the effect of adding *hly-M2* was negligible (Figures 5B and 5D). For the *prsA2-M1* mutant, we observed the reverse situation: addition of *hly-M2* (but not *hly*) caused significantly stronger inhibition of RNase J1 activity compared with the WT *hly* transcript (Figures 5C and 5D). Collectively, these data suggest that *hly* binding increases *prsA2* stability by protecting it from degradation by RNase J1, and that the interaction sites in the *hly* 3′ UTR and *prsA2* 5′ UTR are required for this protection. Despite undertaking several strategies, we have been unable to create a *L. monocytogenes*

strain lacking RNase J1. Although RNase J1 is not essential in *B. subtilis*, it has been shown to be essential in some Gram-positive bacteria (Bugrysheva and Scott, 2010).

The *hly-prsA2* Interaction Is Important for *L. monocytogenes* Pathogenicity

PrsA2 is an important virulence factor, and a *L. monocytogenes* strain lacking PrsA2 is severely attenuated during infection (Alonzo and Freitag, 2010; Alonzo et al., 2009, 2011; Cahoon and Freitag, 2015; Cahoon et al., 2016; Port and Freitag, 2007; Zemansky et al., 2009). To examine whether the *hly-prsA2* interaction is required for infectivity, we first monitored our set of strains (WT, M1, M2, and M1+M2) in a plaque assay, where the ability of the bacteria to spread from cell to cell is monitored (Sun et al., 1990). The M1 and M2 mutant strains lacking a functional *hly-prsA2* interaction showed a significantly reduced capacity to spread between cells as compared with the WT and M1+M2 strains (Figures 6A and 6B). In line with the results from the plaque assay, the M1 and M2 strains were attenuated (2–3 orders of magnitude) in their ability to colonize the liver and spleen in mice compared with the WT strain (Figure 6C). It should be noted that strains completely lacking PrsA2 exhibit more severe infection attenuation in comparison with the levels observed for the M1 and M2 mutants (Alonzo and Freitag, 2010; Alonzo et al., 2009, 2011; Cahoon and Freitag, 2015; Cahoon et al., 2016; Port and Freitag, 2007; Zemansky et al., 2009). This suggests that the residual PrsA2 expressed in the M1 and M2 mutants (~30% of WT) provides some measure of chaperone activity that contributes to infection. The double-mutant M1+M2 strain showed a significantly enhanced ability to colonize the liver and spleen compared with the M1 and M2 single-mutant strains, although in contrast with the full complementation observed for the plaque assay, full virulence was not restored. This could indicate that either the 5′ UTR of *prsA2* or the 3′ UTR of *hly* may interact with additional targets that are critical for mouse infection, or alternatively, that the slightly lower levels of PrsA2 in the M1+M2 strain cause the phenotype. In a *prfA** background, the lack of a functional *hly-prsA2* interaction was even more detrimental for *L. monocytogenes* pathogenicity. The ability of the M1 PrfA* and M2 PrfA* mutant strains to spread from cell to cell and to colonize the liver and spleen of mice was reduced significantly compared with the PrfA* strain alone (Figures S6A–S6C). Overall, our data suggest that a direct *hly-prsA2* interaction is required for *L. monocytogenes* infectivity.

The genus *Listeria* contains 20 species. Of these, only three are hemolytic and encode LLO (*L. monocytogenes*, *L. ivanovii*, and *L. seeligeri*). To examine whether the *hly-prsA2* interaction was conserved in these strains, we compared the 3′ UTRs of *hly* (Figures 6D and S6D). The region of the *hly* 3′ UTR that interacts with *prsA2* in *L. monocytogenes* is conserved in *L. ivanovii* and *L. seeligeri*. This is especially evident for the region interacting with the extreme 5′ end of *prsA2*, strongly suggesting that the *hly-prsA2* interaction is also functionally important in other hemolytic *Listeria* species (Figure S6D).

DISCUSSION

The action of regulatory RNAs is often based on dynamic changes in base-pairing interactions. We employed this principle to search for novel regulatory RNAs in the human pathogenic bacterium *L. monocytogenes*. The recent development of high-throughput

approaches for RNA structure probing made it possible to simultaneously compare RNA structures for multiple transcripts. However, the functional changes of RNA structure can be small (Meyer et al., 2017), and their detection can require very high sequencing coverage. Because the 5′ UTRs have been shown to be an important regulatory region, we focused on the structures of the 5′ ends of bacterial mRNAs and used an enrichment protocol that increases their sequencing coverage. A conceptually similar approach has previously been used to selectively profile the structure of eukaryotic 3′ UTRs (Wu and Bartel, 2017).

Comparison of DMS reactivities at different temperatures uncovered a structural rearrangement in the 5′ UTR of an mRNA encoding the major cold shock protein CspA. When the temperature increases, the *cspA* 5′ UTR rearranges from the “open” to “closed” conformation, and its ribosome-binding site becomes occluded in a hairpin. Our study suggests that this new element acts as an RNA thermoswitch that inhibits *cspA* translation when the temperature increases to above ~30°C. A functionally similar RNA thermoswitch has previously been discovered in *E. coli*, where it also regulates translation of the *cspA* mRNA (Figure S3E; Giuliodori et al., 2010; Zhang et al., 2018). In *E. coli* and *S. aureus*, the *cspA* 5′ UTR also plays a role in autoregulation of CspA expression. In *E. coli*, the CspA protein binds to the 5′ UTR of its own mRNA and shifts the equilibrium to a conformation that inhibits translation (Zhang et al., 2018). In *S. aureus*, RNase III increases translation of the *cspA* mRNA by cleaving a hairpin in its 5′ UTR. CspA binds and unwinds a U-rich motif in the hairpin, thus interfering with RNase III cleavage and leading to inhibition of *cspA* translation (Caballero et al., 2018). A similar autoinhibitory loop might exist in *L. monocytogenes*: the U-rich motif that participates in formation of the hairpin in the open conformation might represent an attractive target for CspA binding (Figure 3A). The unwinding of this hairpin would shift the structure equilibrium to the closed conformation.

The other regulatory events we detected in our study involved the base-pairing of two independent transcripts to each other. When studying how the deletion of the RNA chaperone Hfq affects RNA structure, we detected a “footprint” in the *lmo0850* mRNA. The LhrA-*lmo0850* interaction has been thoroughly studied before, showing that LhrA blocks ribosome binding to the SD in a Hfq-dependent manner (Nielsen et al., 2010). Previously, the footprints of sRNAs on their targets have almost exclusively been demonstrated *in vitro* (Mollerup et al., 2016; Sharma et al., 2007). The detection of an interaction between two RNAs *in vivo* suggested that RNA structure profiling can help to discover novel *trans*-acting regulatory RNAs. The structure probing method provides orthogonal information about interactions between RNA molecules and can be used to complement other methods to search for novel *trans*-acting (small) RNA targets. The traditional approaches to search for the targets of sRNAs in bacteria include genetic screens (Vogel and Sharma, 2005), mutation analysis or overproduction of sRNAs, and studying how this affects the transcriptome or proteome (Borgmann et al., 2018; Nielsen et al., 2011). They also include bioinformatics approaches (Pain et al., 2015). More recently developed approaches are based on pull-down of proteins mediating RNA-RNA interactions followed by proximity ligation and high-throughput sequencing of the hybrid fragments (Melamed et al., 2016; Waters et al., 2017). Proximity ligation methods have proved useful to detect novel (and unexpected) RNA-RNA interactions.

In this work, we also discovered an interaction between two mRNAs, through the detection of a “footprint” that appeared on the *prsA2* 5′ UTR upon activation of the *L. monocytogenes* virulence program (Figures 4, 5, and S5). This was followed by bioinformatics search for transcripts predicted to form base pair interactions with this footprint, with the 3′ UTR of the full-length *hly* transcript showing the best match. Most *trans*-acting RNAs discovered in bacteria represent short transcripts. Although some of them code for polypeptides, typically their length does not exceed 80 amino acids (Raina et al., 2018). Currently, there is only one example of a “classical” mRNA acting *in trans* to regulate expression of another mRNA: the 5′ UTR of the relatively short *irvA* mRNA (~520 nt) from *S. mutans* base pairs with the coding region of *gbpC* mRNA and protects it from RNase J2 degradation (Liu et al., 2015). In this study, we expand the repertoire of described mRNA-mRNA interactions by showing that in *L. monocytogenes* the 3′ UTR of the full-length *hly* transcript directly binds the 5′ UTR of *prsA2* mRNA, protecting it from degradation by RNase J1 (and perhaps other RNases), thereby increasing PrsA2 chaperone production (Figure 7). Surprisingly, even the low amount of *hly* mRNA expressed in non-virulence conditions is sufficient to stabilize the *prsA2* transcript, suggesting a role for the *hly* transcript also outside the host.

It is intriguing to speculate that the *hly-prsA2* mRNA interaction may serve to couple translation and secretion of the two proteins, thereby potentially providing readily available PrsA2 for LLO folding. So far, most 3′ UTRs with a regulatory role have been shown to act as individual sRNAs, through processing from the full-length mRNA or by having an ORF-internal promoter (Miyakoshi et al., 2015). Here, we have identified a regulatory 3′ UTR that remains attached to its coding sequence. Because the LLO and PrsA2 proteins interact, in this case it would make sense that the 3′ UTR remains attached to the *hly* transcript so that the *hly* and *prsA2* transcripts stay associated with each other to facilitate the interaction of their products.

It was unexpected that only a 3-fold reduction in PrsA2 levels would have such a strong impact on *L. monocytogenes* virulence. However, although the results from plaque assays indicate full restoration of cell-to-cell spread in the M1+M2 double mutant, it was apparent that the strain bearing complementary mutations in both the 3′ UTR of *hly* and the 5′ UTR of *prsA2* did not fully restore virulence in mice to the WT levels (although virulence was significantly increased in comparison with the single mutants). We therefore considered the possibility that *hly* might have other (PrfA-regulated) targets than *prsA2* or vice versa, especially because we were unable to create a M1-M2 double mutant in the PrfA* background. The only obvious binding candidate for the *prsA2* mRNA was *hly* (Table S5). However, when examining for possible targets of the *hly* 3′ UTR that could explain the phenotype, one significant candidate appeared that had a stronger binding score than *prsA2*: the transcriptional termination region of *lmo2494* (Table S5). This region also involves an antisense RNA, Rli142, which overlaps the terminator of *lmo2494* (Wurtzel et al., 2012). *lmo2494* encodes the phosphate uptake regulator PhoU and is part of an operon encoding proteins important for phosphate uptake (*pstSCAB-phoU*). Phosphate uptake has been shown to be important for *Salmonella* pathogenicity, and its regulation also involves an antisense RNA, AmgR, that targets the virulence-associated protein MgtC (Lee and Groisman, 2010). Expression of the genes in the *pstSCAB-phoU* operon is upregulated in the intestine in a SigB- and PrfA-dependent manner (Toledo-Arana et al., 2009), but do

not have an obvious PrfA-box. Interestingly, the suggested interaction site in *hly* overlaps with the *prsA2* binding site by 11 bases. Further work is required to define whether the expression of the *lmo2494* operon is controlled by *hly* and/or whether phosphate uptake might be important for virulence.

Although we did not comprehensively assess the performance of our 5′ UTR enrichment strategy, it allowed us to discover functional elements by sequencing DMS-MaPseq libraries of moderate size (≈10 million sequencing reads). Because *lmo0850* and *prsA2* are expressed only at low levels, the 5′ UTR enrichment was necessary to observe differences in DMS reactivity between different conditions. Larger libraries would increase the depth and might aid in the identification of more complex regulatory events. Also, the datasets obtained by FUSE in different conditions stems from few replicates. Despite this, we were able to confirm the discoveries made by FUSE using other methods.

In summary, we have identified RNA regulatory interactions through the targeted structural analyses of *L. monocytogenes* 5′ UTRs *in vitro* and *in vivo*. As exemplified in this and other studies, different MaP-seq methods can be used to identify both intragenic and intergenic RNA-RNA interactions, and we consider FUSE to be an excellent screening approach that requires further analysis to reveal details of mechanisms. Hence such approaches will be very fruitful to reveal new hidden RNA-based mechanisms.

STAR★METHODS

LEAD CONTACT AND MATERIALS AVAILABILITY

Further information and resource requests should be directed to and will be fulfilled by the Lead Contact, Jörgen Johansson (jorgen.johansson@umu.se). This study did not generate new unique reagents.

EXPERIMENTAL MODEL AND SUBJECT DETAILS

Bacterial strains and growth conditions—For cloning purposes and reporter gene assay we used *E. coli* strain DH5a, which was grown in LB medium at constant shaking. For RNA structure profiling and other experiments *L. monocytogenes* EGDe strain and its mutants (Table S8) were used. Before each experiment *L. monocytogenes* cells were grown overnight in BHI medium (BD Biosciences) at 37°C and constant shaking. For structure probing, the bacteria were diluted 1:100 in 25 mL fresh BHI and grown to OD_{600} = 1.0. Growth was followed using a spectrophotometer (Amersham Biosciences).

For the experiments requiring induction of PrfA virulence regulator, *L. monocytogenes* cells were diluted 1:100 in 25 mL of the Activation medium: 1x LB broth buffered with 50 mM MOPS pH = 7.3 and supplemented with 25mM glucose-1-phosphate and 1% Amberlite XAD4 resin (Sigma-Aldrich) (Ermolaeva et al., 2004; Ripio et al., 1997). As a negative control of the Activation medium, the bacteria were grown in 1x LB broth. The cultures were grown at constant shaking at 37°C for 5 hours until early stationary growth phase.

Cell lines—Mouse L2 fibroblasts were cultivated in DMEM + 5% Fetal bovine serum at 37°C in the 5% CO_2 incubator. For performing the plaque assay, 2×10^6 L2 cells per well were seeded into 6-well plates and grown for 16 h before infection with *L. monocytogenes*.

Animal studies—Animal procedures were approved by the University of Illinois at Chicago Animal Care Committee and were conducted in the Biological Resources Laboratory. For infection studies female 7–9-week-old Swiss Webster mice (Charles River Laboratories) were administered 200μL containing 2×10^4 CFU of bacteria by tail vein injection. The experimental groups consisted of randomly assigned littermates.

METHOD DETAILS

RNA isolation—10 mL of bacterial culture was mixed with 2 mL of 1:20 phenol:ethanol solution and centrifuged at 7000 g for 10 minutes. The pellet was resuspended in Disruption solution (10% glucose, 12.5 mM Tris-HCl pH 7.6, and 5 mM EDTA) and immediately transferred to 2 mL screw-capped tubes with roughly 0.4 g glass beads and 500 μL of acid phenol (pH 4.5). The bacteria were disrupted using a mini bead beater (Biospec products) for 30 s. After centrifugation (5 min, 12000 g) RNA was recovered by addition of 1 mL of TRI Reagent Solution (Thermo Fisher) and 100 μL of chloroform, followed by centrifugation. Samples were thereafter subjected to two additional chloroform extractions. The aqueous phase was precipitated by adding isopropanol (0.7 ×) and incubation at −20°C for 20 min. For collection of the pellet, the RNA samples were centrifuged for 25 min. The pellet was washed with 80% ethanol and dissolved in 50 μL of RNase-free water.

Treatment of L. monocytogenes cells and RNA with dimethyl sulfate—*L. monocytogenes* cells (Table S1) were grown overnight in BHI media at 37°C and constant shaking. The stationary phase cultures were diluted 1:100 in a fresh BHI buffered with 50 mM MOPS pH = 7.3 and grown with constant shaking at 26°C or 37°C until OD_{600} = 1 (mid-logarithmic growth phase). Three milliliters of cells were put at 37°C or 26°C in a thermostat and treated with 3% and 5% dimethyl sulfate (DMS) solution respectively for 3 minutes under constant mixing. DMS was inactivated by adding 6 mL of Quenching solution (50% isoamyl alcohol and 30% β-mercaptoethanol). The cells were centrifuged and washed with 10 mL of 30% β-mercaptoethanol. The pellet was resuspended in Disruption solution and RNA was isolated. For *in vitro* treatment with DMS, RNA was isolated from *L. monocytogenes* cells grown at the same conditions. 5 μg of RNA was denatured in mQ water and folded at 37°C for 30 min in 300 μL Folding buffer (50 mM HEPES, 100 mM KCl, 6 mM $MgCl_2$). RNA was treated at 37°C with 3% DMS solution for 3 minutes. DMS was inactivated by adding 300 μL of 30% β-mercaptoethanol and RNA was ethanol precipitated.

FUSE libraries—After modification with DMS, RNA was treated with DNase I (Roche) and purified on RNeasy MinElute columns (QIAGEN). RNA was treated with RNA 5′ Polyphosphatase (Epicenter) and once again purified on the columns. RNA was depleted of ribosomal fraction with Ribo-Zero rRNA Removal Kit (Illumina), and purified on RNeasy columns. The RNA solution was concentrated on a SpeedVac Concentrator (ThermoFisher Scientific) to 4.5 μl, mixed with 1 μl of 15 μM PAGE-purified 5′ RA (RNA adaptor; Table S6), heated for 3 min at 65°C and cooled on ice. The ligation reaction was assembled with

T4 RNA Ligase 1 (NEB) and 10% DMSO, and incubated for 2 hours at room temperature. RNA was ethanol precipitated, dissolved in 9 μl of mQ water and fragmented with RNA Fragmentation Reagents (Thermo Fisher Scientific) for 3.5 min at 70°C. Following the fragmentation, RNA was run on 6% denaturing polyacrylamide gel, and fragments ranging in size from 125 to 400 nucleotides were isolated from the gel. RNA fragments were dephosphorylated with T4 Polynucleotide Kinase (Thermo Fisher Scientific) in the dephosphorylation buffer (100 mM MES pH6.0, 10 mM $MgCl_2$) and purified on RNeasy columns according to a modified protocol (100 μL of RNA solution was mixed with 350 μL RLT buffer and 550 μL 96% ethanol). The modified protocol preserves fragments shorter than 200 nucleotides and is used at the steps following RNA fragmentation. 3′ DA (DNA adaptor) was adenylated with a 5′ DNA Adenylation Kit (NEB). The RNA solution was concentrated to 4.5 μL and mixed with 1 μl of 15 μM adenyl-3′ DA. The ligation reaction with truncated T4 RNA Ligase 2 (NEB) and 25% PEG-8000 was allowed to proceed for 2 hours at room temperature. RNA was ethanol precipitated, dissolved in 20 μL of mQ water and treated with 1.6x vol:vol AMPure XP beads (Beckman Coulter) to remove non-ligated adaptors. cDNA was synthesized with TGIRTIII enzyme (InGex): the RNA solution was concentrated to 4.5 μl, mixed with 1 μl of1 μM RT primer and heated for 2 min at 80°C. The primer was annealed for 5 minutes at room temperature, and the reverse transcription reaction was assembled in RT buffer (50 mM Tris-HCl pH8.3, 75 mM KCl, 3 mM $MgCl_2$) with 1 mM dNTPs mix, 5 mM DTT and 100U of TGIRTIII enzyme. The reverse transcription was incubated for 2 hours at 57°C. After that 1 μl of 5N NaOH was added to the reaction and the reverse transcriptase was inactivated by heating at 95°C for 3 min. The first strands of cDNA were ethanol precipitated, dissolved in mQ water and cDNA libraries were amplified by 20 rounds of PCR. The first 12 cycles of PCR were performed with primers LibAmp_F and LibAmp_RPIXX_R, which introduced sequences identical to Illumina TruSeq adapters (Oligonucleotide sequences © 2018 Illumina, Inc. All rights reserved) to cDNA. The product of the first PCR reaction was purified with 1x vol:vol AMPure XP beads and used as the matrix for the second 6–8 cycles PCR reaction with primers Enrich_F and Enrich_R. The product of the second PCR reaction was sequentially purified with RNeasy PCR Purification Kit (QIAGEN) and 1x vol:vol AMPure XP beads. The resulting libraries were sequenced on Illumina sequencing platform in 2 × 76 bp paired-end mode.

The whole-transcriptome DMS-MaPseq libraries—To prepare DMS-MaPseq libraries without 5′ UTR enrichment, RNA was depleted of ribosomal fraction with Ribo-Zero rRNA Removal Kit (Illumina), and purified on RNeasy columns. RNA was fragmented with RNA Fragmentation Reagents (Thermo Fisher Scientific) for 3.5 min at 70°C, and purified on RNeasy columns according to the modified protocol (100 μL of RNA solution was mixed with 350 μL RLT buffer (QIAGEN) and 550 μL 96% ethanol). RNA fragments were dephosphorylated with Shrimp Alkaline Phosphatase (NEB), purified on RNeasy columns according to the modified protocol, 5′ phosphorylated with T4 Polynucleotide Kinase (NEB), and once again purified on the columns according to the modified protocol. RNA solution was concentrated to 4.5 μl, mixed with 1 μl of 15 μM PAGE purified 5′RA, heated for 3 min at 65° C and cooled on ice. The ligation reaction was assembled with T4 RNA Ligase (NEB) and 10% DMSO, and incubated for 2 hours at room temperature. RNA

was ethanol precipitated, run on a 6% denaturing polyacrylamide gel, and fragments ranging in size from 100 to 400 nucleotides were isolated from the gel. Adenylated 3′ DA adaptor was ligated to the RNA fragments with truncated T4 RNA Ligase 2 (NEB) in the presence of 25% PEG-8000 for 2 hours at room temperature. RNA was treated with 1.6x vol:vol AMPure XP beads (Beckman Coulter) to remove unligated adaptors. cDNA was synthesized with TGIRTIII enzyme, amplified and purified exactly the same as for the 5′ UTR-enriched libraries. The resulting libraries were sequenced on Illumina sequencing platform in 2 × 76 bp paired-end mode.

Targeted DMS-MaPseq of prfA 5′ UTR—*L. monocytogenes* EGDe cells grown at 26°C or 37°C were treated with DMS and used for RNA isolation as described in the respective section of Methods. Total RNA was depleted of rRNA using Ribo-Zero rRNA Removal Reagent for Gram-positive bacteria (Illumina). Specific cDNA was synthesized with TGIRTIII reverse transcriptase (InGex) using 10 μM primer prfA_RT (Table S6). The region of *prfA* 5′ UTR was amplified with primers prfA_DMS_F and prfA_DMS_R. Indexes for both amplicons were added by PCR amplification using primers LibAmp_F and LibAmp_RPI#_R (with a unique index). The libraries were further enriched by PCR using Enrich_F and Enrich_R primers as described for FUSE or the whole-transcriptome DMS-MaPseq in the respective section of STAR Methods.

Reporter gene assay—The region comprising *lmo1364 (cspA)* 5′ UTR and the first 10 codons was amplified from *L. monocytogenes* EGD-e genome with primers cspA_NheI_F and cspA_EcoRI_R (Table S6) and cloned into pBAD2-bgaB vector (Klinkert et al., 2012). The 5′ UTRs and the first codons of the genes *lmo0277*, *lmo0354* and *lmo2110* were cloned into pBAD2-bgaB in the same manner. Mutations were introduced to the cloned *cspA* 5′ UTR sequence by inverse PCR with back-to-back primers cspA_M1/2/3/4_F and cspA_M1/2/3/4_R. The pBAD2-bgaB-5′ UTR plasmids (Table S8) were introduced to *E. coli* DH5α. Cells were grown at 26°C in LB medium supplemented with ampicillin (150 mg/L) to OD_{600} = 0.5. Transcription was induced by adding 0.01% arabinose, and half of each culture was transferred to 37°C. After 30 minutes of induction, 1 mL of cultures were harvested and β-galactosidase activity was measured as described (Gaubig et al., 2011).

Native PAGE of *in vitro* folded cspA 5′ UTR—Matrices for *in vitro* transcription were amplified from the plasmids pBAD2-bgaB containing *cspA* 5′ UTR and its mutated forms with primers cspA_T7_F and cspA_T7_R (Table S6). *In vitro* transcription was performed with MAXIscript T7 Transcription Kit (Thermo Fisher Scientific) and the synthesized RNA was purified on 6% denaturing polyacrylamide gel (19:1 acrylamide/bis-acrylamide ratio). To study the effect of temperature on folding, 50 ng of *cspA* 5′ UTR was dissolved in 9 μL of Loading buffer (10 mM Tris-HCl pH7.0, 1 mM EDTA, 10% glycerol, 0.01% xylene cyanol), denatured at 95°C for 3 minutes and quickly cooled on ice. To initiate refolding, 1 μl of 500 mM NaCl solution was added, and RNA was incubated at temperatures ranging from 26°C to 37°C for 5 minutes. The folded RNA was applied to the 10% acrylamide gel containing 100 mM Tris-HEPES (pH = 7.5), 0.1 mM EDTA, 3 mM $MgCl_2$, and run at 4°C with a running buffer of the same composition. The RNA fragments in the gel were visualized by staining with SYBR Gold stain (Thermo Fisher Scientific).

DMS-MaPseq of *in vitro* folded cspA 5′ UTR—Template for *in vitro* transcription of *cspA* 5′ UTR was generated by PCR-amplification using primers cspA_T7_F and cspA_T7_R (Table S6). *cspA* 5′ UTR was produced using MEGAscript T7 Transcription kit and gel purified from 6% denaturing polyacrylamide gel (19:1 acrylamide/bis-acrylamide ratio). RNA was concentrated by ethanol precipitation and equilibrated to a desired buffering solution using gel filtration on PD SpinTrap G-25 columns (GE).

cspA 5′ UTR was dissolved to a final concentration of 5.6 ng/μl in 10 mM MOPS-Na pH 7.0, 1 mM EDTA and 10% (w/vol) glycerol (90 μl). RNA was denatured for 3 minutes at 95°C and cooled on ice. Folding was initiated by adding NaCl to a final concentration of 50 mM (100 μL final volume) and equilibrating temperature to either 26 or 37°C for 10 minutes. DMS was added at 5% and 3% (vol/vol) for 26°C and 37°C samples respectively, and incubated for 3 minutes. DMS was quenched by adding 50 μL 2-mercaptoethanol, RNA was ethanol precipitated and further processed for sequencing library preparation as described in FUSE protocol.

Creation of L. monocytogenes mutants—The genome fragment encompassing the 5′ UTR of *prsA2* gene as well as 606 and 811 nucleotides upstream and downstream of the 5′ UTR was amplified from *L. monocytogenes* EGD-e genome with primers UTR2219_loc_NcoI and UTR2219_loc_SalI (Table S6). Similarly, the genome locus of the 3′ UTR of *hly* gene was amplified with primers UTR0202_loc_NcoI and UTR2219_-loc_SalI. The fragments were digested with *Nco*I and SalI restriction enzymes and cloned to pMAD vector digested with the same enzymes (Arnaud et al., 2004). Mutations were introduced to the cloned fragments by inverse PCR with primers UTR0202_mut_F and UTR0202_mut_R, and UTR2219_mut_F and UTR2219_mut_R. The resulting vectors (Table S8) were introduced to *L. monocytogenes* EGD-e cells by electroporation. The mutants (Table S1) were generated according to the procedure described in Arnaud et al. (2004) and the loci later sequenced to assure that the mutations had been introduced on the chromosome.

Quantitative RT-PCR—*L. monocytogenes* EGD-e cells were grown overnight in BHI media at 37°C and constant shaking. The stationary phase cultures were diluted 1:100 in the Activation media: 1x LB broth buffered with 50 mM MOPS pH = 7.3 and supplemented with 25mM glucose-1-phosphate and 1% Amberlite XAD4 resin (Sigma-Aldrich) (Ermolaeva et al., 2004; Ripio et al., 1997). The culture was grown at constant shaking at 37°C for 5 hours until early stationary growth phase. RNA was isolated from cells. 1 μg of RNA was treated with DNase I (Roche) and purified on RNeasy MinElute columns (QIAGEN). cDNA synthesis was performed with RevertAid First Strand cDNA Synthesis Kit (Thermo Fisher Scientific). The levels of *hly* and *prsA2* mRNAs were measured by quantitative RT-PCR with respective primers (Table S6) and normalized to the level of 16S rRNA. Quantitative RT-PCR was performed with Maxima SYBR Green qPCR Master Mix (Thermo Fisher Scientific).

Western blotting—*L. monocytogenes* EGDe strain and its derivatives with M1, M2 and M1+M2 mutations (Table S1) were grown in LB medium supplemented with 50 mM MOPS-Na pH 7.3 (non-inducing conditions), or same medium with addition of 25 mM

Glucose-1-Phosphate and 1% (w/vol) Amberlite XAD4 (virulence inducing conditions). After 5 hours of growth, the secreted and cellular protein fractions were prepared. The secreted protein fraction was prepared according to Netterling et al. (2015): the bacterial culture supernatant was harvested and filtered through 0.22 μm PVDF filter (Millipore). Next, 1 mL of supernatant was mixed with 10 μL of 2% sodium deoxycholate (Sigma-Aldrich) and incubated for 10 min at room temperature before precipitation with 250 μL of 50% trichloroacetic acid (Sigma-Aldrich) on ice for 1 h. After centrifugation at 20000 × *g* at 4°C for 30 min, the supernatant was removed, and the pellet was resuspended in 580 μL of 80% ice-cold acetone. The suspension was centrifuged at 20800 × *g* at 4°C for 30 min before the pellet was dried and resuspended in 15 μL of 1x Laemmli sample buffer (62.5 mM Tris-HCl pH 6.8, 2% SDS, 10% glycerol, 5% β-mercaptoethanol, 0.001% bromophenol blue).

Preparation of the cellular protein fraction was performed according to the following protocol: 600 μL of culture was mixed with 600 μL of 1:1 acetone:ethanol solution, incubated on ice for 10 min and centrifuged at 20,800 × *g* for 5 min. The pellet was washed two times with 500 μL of wash buffer (30 mM Tris-HCl pH 8.0, 50 mM NaCl, 5 mM EDTA), resuspended in 45 μL of Mutanolysin mix: 50 mM Tris-HCl (pH 6.8), Mutanolysin (0.1 U/μl) and DNase (0.2 U/μl), and incubated at 37°C for 1 h. Afterward, 15 μL of 4x Laemmli buffer (250 mM Tris-HCl pH 6.8, 8% SDS, 40% glycerol, 20% β-mercaptoethanol, 0.004% bromophenol blue) was added, the sample was heated for 30 min at 95°C and centrifuged at 20,800 × *g* for 5 min.

After isolation, the protein fractions were separated on 12% SDS-polyacrylamide gels and transferred to the BioTrace NT Nitrocellulose Transfer Membrane (Pall) using Trans-Blot Turbo Transfer System (Bio-Rad). Membranes were blocked in 5% dry milk. To detect LLO levels, the membrane with the secreted protein fraction was incubated with primary polyclonal anti-LLO antibody (Abcam) diluted 1:2500. The level of p60 protein in the secreted fraction was detected with the polyclonal antibodies diluted 1:3000 (Netterling et al., 2015). To detect PrsA2 levels, the membrane with the intracellular proteins fraction was incubated with primary polyclonal anti-PrsA2 antibody diluted 1:2500 (Alonzo et al., 2009). The level of ActA protein in the intracellular fraction was detected with the polyclonal antibodies diluted 1:4000 (Netterling et al., 2015). Membranes were washed and incubated with anti-rabbit-horseradish peroxidase secondary antibody (Agrisera), diluted 1:10000. The expression levels of each protein (the intensity of chemiluminescence) were detected and measured using a LAS4000 image analyzer (Fuji). The Coomassie stained gel served as a loading control for PrsA2 expression levels, and the expression of LLO was normalized to the area under the growth curves of the bacterial cultures.

Northern blotting—10 μg of RNA was separated on a formaldehyde agarose gel as described in Durand et al. (2015) and transferred to the Hybond-N membrane (GE Life Sciences) by the capillary transfer according to the manufacturer's protocol. The RNA was UV cross-linked to the membrane with Spectrolinker XL-1000 machine (Spectroline). The oligonucleotides complementary to *hly* mRNA CDS and 3′ UTR, Rli51 and tmRNA (Table S6) were labeled with $\gamma-^{32}$P ATP using T4 polynucleotide kinase (Thermo Fisher Scientific) and hybridized with the membrane in the Rapid-hyb buffer (GE Life Sciences).

The radioactive signal was detected with a storage phosphor screen and Typhoon FLA 9500 laser scanner (GE Life Sciences).

Measurement of prsA2 mRNA stability—*L. monocytogenes* EGDe strain and its derivatives with M1, M2 and M1+M2 mutations (Table S1) were grown in LB medium supplemented with 50 mM MOPS-Na pH 7.3 (non-inducing conditions), or same medium with addition of 25 mM Glucose-1-Phosphate and 1% (w/vol) Amberlite XAD4 (virulence inducing conditions). At culture density of OD_{600} = 0.5 a 1 mL sample was mixed with 200 μL of 5% (w/vol) phenol in ethanol (time point 0). Rifampicin was added to bacterial cultures to a final concentration of 250 μg/ml and samples were taken the same way after 2, 5 and 10 minutes. Bacteria were collected by centrifugation for 5 minutes at 10000 × g and pellets kept frozen at −80°C for further processing.

Total RNA was isolated using Direct-zol RNA Miniprep Kit (Zymo Research). Northern blotting was performed as described in the respective section of Materials and Methods. Briefly, 4 μg/well of RNA was run in denaturing agarose gel, transferred onto a Hybond-N (GE) membrane, which was then hybridized with 5′^{32}P labeled oligonucleotide probes lmo2219-oligoprobe and tmRNA_probe. The bands corresponding to *prsA2* (*lmo2219*) and tmRNA transcripts were detected by exposing membranes to a storage phosphorscreen (GE) and scanning with a Typhoon FLA9500 (GE). Quantification was done using ImageJ ROI Measurement tool, *prsA2* signals were normalized to tmRNA levels.

RNase J1 assays—The 53-nt *prsA2* and *prsA2-M1* RNA fragments were transcribed *in vitro* from PCR fragments containing the 5′ UTR and the first 6 nucleotides of the *prsA2* coding sequence. The *prsA2* and *prsA2-M1* templates were amplified using *L. monocytogenes* chromosomal DNA and oligo pairs 5UTR2219_rnj_F / 5UTR2219_rnj_R and 5UTR2219_M1_rnj_F / 5UTR2219_rnj_R, respectively. The *hly* and *hly-M2* templates were amplified by PCR using oligos 3UTR0202_rnj_F / 3UTR0202_rnj_R and 3UTR0202_M2_rnj_F / 3UTR0202_rnj_R, respectively. The *prsA2* and *prsA2-M1* RNAs were dephosphorylated with Calf Intestinal Phosphatase (CIP) (10 U/ml; Biolabs) and 5′ end-labeled with T4 polynucleotide kinase (PNK) and [γ−^{32}P]-ATP. The *prsA2* and *prsA2-M1* RNAs (10 pmol) were pre-heated 5 min in a 95° C water bath with or without *hly* or *hly-M2* (20 pmol), and cooled to 4°C. Then, the appropriate volume of 5x J1 buffer (100 mM Tris pH 6.8, 40 mM $MgCl_2$, 500 mM NH_4Cl, 0.5 mM DTT) was added for n+1 5 μL reactions. The reaction mixture was incubated at 37°C. 5 μL of reaction mix was stopped with 5uL RNA loading dye (Ambion) before (time 0) and 2.5, 5 and 10 min after addition of RNase J1 (0.8 μg per 5 μL reaction) at 37°C (Mathy et al., 2007). The *prsA2* and *prsA2-M1* RNAs were also incubated without RNase J1 for 10 min at 37°C.

L. monocytogenes infection of mice—Animal procedures were approved by the University of Illinois at Chicago Animal Care Committee and were conducted in the Biological Resources Laboratory. Saturated overnight cultures of *L. monocytogenes* EGDe were diluted 1:20 in BHI broth, grown to mid-log phase and normalized based on OD_{600} values. Bacteria were washed twice and re-suspended in PBS pH 7. Female 7–9-week-old Swiss Webster mice (Charles River Laboratories) were administered 200μL containing 2×10^4 CFU of bacteria by tail vein injection. At 72 hours post infection, organs of infected

animals were collected, homogenized, and 10-fold serial dilutions were plated for total CFUs.

Plaque assay—Plaque assays were conducted as previously described (Sun et al., 1990). Briefly, monolayers of L2 fibroblasts in 6-well culture dishes were infected at an MOI of 30:1 for 1 hour. Then infected monolayers were washed three times with PBS pH 7 and overlaid with DMEM/agarose containing 10 μg/ml gentamicin to kill extracellular bacteria. Plaques were measured at 72 hours with a micrometer.

QUANTIFICATION AND STATISTICAL ANALYSIS

Analysis of DMS-MaPseq and FUSE data—The sequencing reads were mapped to *Listeria monocytogenes* EGD-e genome (NC_003210) with Bowtie 2 aligner using the *–end-to-end–very-sensitive* mode (Langmead and Salzberg, 2012). The coordinates of mismatches were extracted from the CIGAR string of the SAM files. The coordinates of transcriptional start sites were obtained from Wurtzel et al. (2012) and verified using our data. Genome regions corresponding to non-coding RNAs, 5′ UTRs and the first 30 nucleotides of coding sequences were selected for further analysis. For each adenine and cytosine nucleotide position of these regions, the coverage was calculated as the number of reads mapped at that position. The mismatch rate (*MR*) of position *i* in sample *j* was calculated as the ratio between the number of mismatches (*mis*) and coverage (*cvg*) at that position:

$$MR_{ij} = \frac{mis_{ij}}{cvg_{ij}}$$

Our DMS treatment conditions resulted in the average mismatch rates for adenine and cytosine nucleotides ranging from 3 to 6% in different samples. In the untreated control, the average mismatch rates for these nucleotides were close to 0.3% (Table S7). The nucleotides with mismatch rate higher than 1% in the untreated control were mostly located in the regions with low sequencing coverage and were excluded from further analysis. To account for variability in DMS treatment conditions of different samples, the mismatch rates of adenines and cytosines were separately divided by the average mismatch rates in the respective sample. The resulting values got the name ‘DMS values’ (Table S3):

$$DMS_{ij} = \frac{MR_{ij}}{\overline{MR}_j}$$

DMS values of each nucleotide were compared between different samples in a pairwise manner. The significance of the differences was estimated by a two-step strategy. At first, we performed Fisher’s exact test. To account for uneven DMS treatment conditions, the number of mismatches at the position *i* and samples 1 and 2 were normalized according to the average mismatch rates in the compared samples:

$$mis^{*}_{i1} = round\left(mis_{i1} * \frac{\overline{MR}_1 + \overline{MR}_2}{2\overline{MR}_1}\right)$$

$$mis^{*}_{i2} = round\left(mis_{i2} * \frac{\overline{MR}_1 + \overline{MR}_2}{2\overline{MR}_2}\right)$$

where $\overline{MR}_j = \overline{MR}^{A}_{j}$ if i corresponds to an adenine positions and $\overline{MR}^{C}_{j}$ otherwise, and the values were rounded to the nearest integers. The normalized number of mismatches and matches were used for the calculation of Fisher's exact test statistics using the following normalized contingency table:

	Sample 1	Sample 2
Number of mismatches at position i	mis^{*}_{i1}	mis^{*}_{i2}
Number of matches at position i	$cvg_{i1} - mis^{*}_{i1}$	$cvg_{i2} - mis^{*}_{i2}$

The calculated *p-value*s were adjusted for multiple comparisons (Benjamini and Hochberg, 1995), and positions with the adjusted *p-value*s < 0.05 were selected for further analysis. Among the statistically significant differences only the differences with a high effect size were regarded as significant. The effect size criterion demanded that the relative difference between the samples' DMS values should be larger than 20% and that the absolute difference between the values should be larger than 0.1. The results of the performed comparisons are represented in Table S4. To discover structural rearrangements, we manually searched for the regions where nucleotides with pronounced changes of DMS reactivity were located close to each other.

Data manipulation was performed with custom Python scripts using HTSeq framework (Anders et al., 2015). Statistical analysis was performed with R scripts, and data visualization with Integrative Genomics Viewer and VARNA software (Darty et al., 2009; Thorvaldsdóttir et al., 2013).

Analysis of quantitative data—We have included the group sizes, number of replicates, statistical tests and significance criteria in figure legends. In most plots the mean and the standard deviation are indicated, and the Student's t test was used for estimation of statistical significance. For the mouse infection data at Figures 6C and S6A the CFU values are presented as boxplots and the statistical significance of differences was estimated with the Wilcoxon Rank-Sum test. The differences were considered significant if *p-value* was less than 0.05.

DATA AND CODE AVAILABILITY

All sequencing data are deposited in NCBI's Gene Expression Omnibus (Barrett et al., 2013). The accession number for the sequencing data reported in this paper is GEO: GSE118387 (https://www.ncbi.nlm.nih.gov/geo/query/acc.cgi?acc=GSE118387). The scripts are deposited at GitHub under the project name 5′-UTR-structure-elucidation' (https://github.com/dimaignatov/5-UTR-structure-elucidation).

ADDITIONAL RESOURCES

There are no additional resources associated with this study.

Supplementary Material

Refer to Web version on PubMed Central for supplementary material.

ACKNOWLEDGMENTS

J.J. was supported by Umeå University, Swedish Research Council grant 2016–03313, the K. A. Wallenberg Foundation, the Wenner-Gren Foundations, Stiftelsen Olle Engkvist Byggmästare, and ERC starting grant 260764-RNAntibiotics. D.I. was supported by the UCMR postdoctoral program. S.D. and C.C. are supported by funds from the CNRS and Université de Paris to UMR 8261, the Agence Nationale de la Recherche (ARNr-QC and BaRR), and the Labex (Dynamo) program (France). L.C. and N.F. were supported by NIH grants R01 AI083241 and AI083241–03S1 to NEF (United States). We are grateful to Drs. A. Le Rhun, L. Broglia, and A. Escalera for critical reading of the manuscript and to Prof. F. Narberhaus (Ruhr University Bochum) for sharing the pBAD2-bgaB plasmid. S. Sondén is acknowledged for technical assistance, and A. Maznina for language editing.

REFERENCES

Alonzo F 3rd, and Freitag NE (2010). Listeria monocytogenes PrsA2 is required for virulence factor secretion and bacterial viability within the host cell cytosol. Infect. Immun. 78, 4944–4957. [PubMed: 20823208]

Alonzo F 3rd, Port GC, Cao M, and Freitag NE (2009). The posttranslocation chaperone PrsA2 contributes to multiple facets of Listeria monocytogenes pathogenesis. Infect. Immun. 77, 2612–2623. [PubMed: 19451247]

Alonzo F 3rd, Xayarath B, Whisstock JC, and Freitag NE (2011). Functional analysis of the Listeria monocytogenes secretion chaperone PrsA2 and its multiple contributions to bacterial virulence. Mol. Microbiol. 80, 1530–1548. [PubMed: 21545417]

Anders S, Pyl PT, and Huber W (2015). HTSeq—a Python framework to work with high-throughput sequencing data. Bioinformatics 31, 166–169. [PubMed: 25260700]

Arnaud M, Chastanet A, and Débarbouillé M (2004). New vector for efficient allelic replacement in naturally nontransformable, low-GC-content, gram-positive bacteria. Appl. Environ. Microbiol. 70, 6887–6891. [PubMed: 15528558]

Barrett T, Wilhite SE, Ledoux P, Evangelista C, Kim IF, Tomashevsky M, Marshall KA, Phillippy KH, Sherman PM, Holko M, et al. (2013). NCBI GEO: archive for functional genomics data sets–update. Nucleic Acids Res. 41, D991–D995. [PubMed: 23193258]

Batey RT, Rambo RP, Lucast L, Rha B, and Doudna JA (2000). Crystal structure of the ribonucleoprotein core of the signal recognition particle. Science 287, 1232–1239. [PubMed: 10678824]

Batey RT, Sagar MB, and Doudna JA (2001). Structural and energetic analysis of RNA recognition by a universally conserved protein from the signal recognition particle. J. Mol. Biol. 307, 229–246. [PubMed: 11243816]

Benjamini Y, and Hochberg Y (1995). Controlling the False Discovery Rate: A Practical and Powerful Approach to Multiple Testing. J. R. Stat. Soc. Ser. B Stat. Methodol. 57, 289–300.

Borgmann J, Schäkermann S, Bandow JE, and Narberhaus F (2018). A Small Regulatory RNA Controls Cell Wall Biosynthesis and Antibiotic Resistance. mBio 9, e02100–e2118.

Bugrysheva JV, and Scott JR (2010). The ribonucleases J1 and J2 are essential for growth and have independent roles in mRNA decay in Streptococcus pyogenes. Mol. Microbiol. 75, 731–743. [PubMed: 20025665]

Burkhardt DH, Rouskin S, Zhang Y, Li GW, Weissman JS, and Gross CA (2017). Operon mRNAs are organized into ORF-centric structures that predict translation efficiency. eLife 6, e22037. [PubMed: 28139975]

Caballero CJ, Menendez-Gil P, Catalan-Moreno A, Vergara-Irigaray M, García B, Segura V, Irurzun N, Villanueva M, Ruiz de Los Mozos I., Solano C, et al. (2018). The regulon of the RNA chaperone CspA and its autoregulation in Staphylococcus aureus. Nucleic Acids Res. 46, 1345–1361. [PubMed: 29309682]

Cahoon LA, and Freitag NE (2015). Identification of Conserved and Species-Specific Functions of the Listeria monocytogenes PrsA2 Secretion Chaperone. Infect. Immun. 83, 4028–4041. [PubMed: 26216425]

Cahoon LA, Freitag NE, and Prehna G (2016). A structural comparison of Listeria monocytogenes protein chaperones PrsA1 and PrsA2 reveals molecular features required for virulence. Mol. Microbiol. 101, 42–61. [PubMed: 27007641]

Chakravarty S, and Massé E (2019). RNA-Dependent Regulation of Virulence in Pathogenic Bacteria. Front. Cell. Infect. Microbiol. 9, 337. [PubMed: 31649894]

Christiansen JK, Larsen MH, Ingmer H, Søgaard-Andersen L, and Kallipolitis BH (2004). The RNA-binding protein Hfq of Listeria monocytogenes: role in stress tolerance and virulence. J. Bacteriol. 186, 3355–3362. [PubMed: 15150220]

Darty K, Denise A, and Ponty Y (2009). VARNA: Interactive drawing and editing of the RNA secondary structure. Bioinformatics 25, 1974–1975. [PubMed: 19398448]

de las Heras A, Cain RJ, Bielecka MK, and Vázquez-Boland JA (2011). Regulation of Listeria virulence: PrfA master and commander. Curr. Opin. Microbiol. 14, 118–127. [PubMed: 21388862]

Di Tommaso P, Moretti S, Xenarios I, Orobitg M, Montanyola A, Chang JM, Taly JF, and Notredame C (2011). T-Coffee: a web server for the multiple sequence alignment of protein and RNA sequences using structural information and homology extension. Nucleic Acids Res. 39, W13–W17. [PubMed: 21558174]

Dos Santos P.T., Menendez-Gil P, Sabharwal D, Christensen JH, Brunhede MZ, Lillebæk EMS, and Kallipolitis BH (2018). The Small Regulatory RNAs LhrC1–5 Contribute to the Response of Listeria monocytogenes to Heme Toxicity. Front. Microbiol. 9, 599. [PubMed: 29636750]

Durand S, Tomasini A, Braun F, Condon C, and Romby P (2015). sRNA and mRNA turnover in Gram-positive bacteria. FEMS Microbiol. Rev. 39, 316–330. [PubMed: 25934118]

Durand S, Braun F, Helfer AC, Romby P, and Condon C (2017). sRNA-mediated activation of gene expression by inhibition of 5′−3′ exonucleolytic mRNA degradation. eLife 6, e23602. [PubMed: 28436820]

Ermolaeva S, Novella S, Vega Y, Ripio MT, Scortti M, and Vázquez-Boland JA (2004). Negative control of Listeria monocytogenes virulence genes by a diffusible autorepressor. Mol. Microbiol. 52, 601–611. [PubMed: 15066044]

Gaubig LC, Waldminghaus T, and Narberhaus F (2011). Multiple layers of control govern expression of the Escherichia coli ibpAB heat-shock operon. Microbiology 157, 66–76. [PubMed: 20864473]

Giuliodori AM, Di Pietro F, Marzi S, Masquida B, Wagner R, Romby P, Gualerzi CO, and Pon CL (2010). The cspA mRNA is a thermosensor that modulates translation of the cold-shock protein CspA. Mol. Cell 37, 21–33. [PubMed: 20129052]

Good JA, Andersson C, Hansen S, Wall J, Krishnan KS, Begum A, Grundström C, Niemiec MS, Vaitkevicius K, Chorell E, et al. (2016). Attenuating Listeria monocytogenes Virulence by Targeting the Regulatory Protein PrfA. Cell Chem. Biol. 23, 404–414. [PubMed: 26991105]

Guo JU, and Bartel DP (2016). RNA G-quadruplexes are globally unfolded in eukaryotic cells and depleted in bacteria. Science 353, aaf5371. [PubMed: 27708011]

Hüttenhofer A, and Noller HF (1994). Footprinting mRNA-ribosome complexes with chemical probes. EMBO J. 13, 3892–3901. [PubMed: 8070416]

Johansson J, Mandin P, Renzoni A, Chiaruttini C, Springer M, and Cossart P (2002). An RNA thermosensor controls expression of virulence genes in Listeria monocytogenes. Cell 110, 551–561. [PubMed: 12230973]

Klinkert B, Cimdins A, Gaubig LC, Roßmanith J, Aschke-Sonnenborn U, and Narberhaus F (2012). Thermogenetic tools to monitor temperature-dependent gene expression in bacteria. J. Biotechnol. 160, 55–63. [PubMed: 22285954]

Langmead B, and Salzberg SL (2012). Fast gapped-read alignment with Bowtie 2. Nat. Methods 9, 357–359. [PubMed: 22388286]

Lebreton A, and Cossart P (2017). RNA- and protein-mediated control of Listeria monocytogenes virulence gene expression. RNA Biol. 14, 460–470. [PubMed: 27217337]

Lee EJ, and Groisman EA (2010). An antisense RNA that governs the expression kinetics of a multifunctional virulence gene. Mol. Microbiol. 76, 1020–1033. [PubMed: 20398218]

Liu N, Niu G, Xie Z, Chen Z, Itzek A, Kreth J, Gillaspy A, Zeng L, Burne R, Qi F, and Merritt J (2015). The Streptococcus mutans irvA gene encodes a trans-acting riboregulatory mRNA. Mol. Cell 57, 179–190. [PubMed: 25574948]

Loh E, Gripenland J, and Johansson J (2006). Control of Listeria monocytogenes virulence by 5′-untranslated RNA. Trends Microbiol. 14, 294–298. [PubMed: 16730443]

Loh E, Dussurget O, Gripenland J, Vaitkevicius K, Tiensuu T, Mandin P, Repoila F, Buchrieser C, Cossart P, and Johansson J (2009). A trans-acting riboswitch controls expression of the virulence regulator PrfA in Listeria monocytogenes. Cell 139, 770–779. [PubMed: 19914169]

Lorenz R, Bernhart SH, Höner Zu Siederdissen C., Tafer H, Flamm C, Stadler PF, and Hofacker IL (2011). ViennaRNA Package 2.0. Algorithms Mol. Biol. 6, 26. [PubMed: 22115189]

MacKaness GB (1964). The Immunological Basis of Acquired Cellular Resistance. J. Exp. Med. 120, 105–120. [PubMed: 14194388]

Masachis S, and Darfeuille F (2018). Type I Toxin-Antitoxin Systems: Regulating Toxin Expression via Shine-Dalgarno Sequence Sequestration and Small RNA Binding. Microbiol. Spectr. 6, RWR-0030–2018.

Mathy N, Bénard L, Pellegrini O, Daou R, Wen T, and Condon C (2007). 5′-to-3′ exoribonuclease activity in bacteria: role of RNase J1 in rRNA maturation and 5′ stability of mRNA. Cell 129, 681–692. [PubMed: 17512403]

McGinnis JL, Liu Q, Lavender CA, Devaraj A, McClory SP, Fredrick K, and Weeks KM (2015). In-cell SHAPE reveals that free 30S ribosome subunits are in the inactive state. Proc. Natl. Acad. Sci. USA 112, 2425–2430. [PubMed: 25675474]

Melamed S, Peer A, Faigenbaum-Romm R, Gatt YE, Reiss N, Bar A, Altuvia Y, Argaman L, and Margalit H (2016). Global Mapping of Small RNA-Target Interactions in Bacteria. Mol. Cell 63, 884–897. [PubMed: 27588604]

Meyer MM (2017). The role of mRNA structure in bacterial translational regulation. Wiley Interdiscip. Rev. RNA 8, e1370.

Meyer S, Carlson PD, and Lucks JB (2017). Characterizing the Structure-Function Relationship of a Naturally Occurring RNA Thermometer. Biochemistry 56, 6629–6638. [PubMed: 29172455]

Miao Z, and Westhof E (2017). RNA Structure: Advances and Assessment of 3D Structure Prediction. Annu. Rev. Biophys. 46, 483–503. [PubMed: 28375730]

Milohanic E, Glaser P, Coppée JY, Frangeul L, Vega Y, Vázquez-Boland JA, Kunst F, Cossart P, and Buchrieser C (2003). Transcriptome analysis of Listeria monocytogenes identifies three groups of genes differently regulated by PrfA. Mol. Microbiol. 47, 1613–1625. [PubMed: 12622816]

Mitchell D 3rd, Assmann SM, and Bevilacqua PC (2019). Probing RNA structure in vivo. Curr. Opin. Struct. Biol. 59, 151–158. [PubMed: 31521910]

Miyakoshi M, Chao Y, and Vogel J (2015). Regulatory small RNAs from the 3′ regions of bacterial mRNAs. Curr. Opin. Microbiol. 24, 132–139. [PubMed: 25677420]

Mizrahi O, Nachshon A, Shitrit A, Gelbart IA, Dobesova M, Brenner S, Kahana C, and Stern-Ginossar N (2018). Virus-Induced Changes in mRNA Secondary Structure Uncover cis-Regulatory Elements that Directly Control Gene Expression. Mol. Cell 72, 862–874.e5. [PubMed: 30318442]

Mollerup MS, Ross JA, Helfer AC, Meistrup K, Romby P, and Kallipolitis BH (2016). Two novel members of the LhrC family of small RNAs in Listeria monocytogenes with overlapping regulatory functions but distinctive expression profiles. RNA Biol. 13, 895–915. [PubMed: 27400116]

Mraheil MA, Billion A, Mohamed W, Mukherjee K, Kuenne C, Pischimarov J, Krawitz C, Retey J, Hartsch T, Chakraborty T, and Hain T (2011). The intracellular sRNA transcriptome of Listeria monocytogenes during growth in macrophages. Nucleic Acids Res. 39, 4235–4248. [PubMed: 21278422]

Mustoe AM, Busan S, Rice GM, Hajdin CE, Peterson BK, Ruda VM, Kubica N, Nutiu R, Baryza JL, and Weeks KM (2018). Pervasive Regulatory Functions of mRNA Structure Revealed by High-Resolution SHAPE Probing. Cell 173, 181–195.e18. [PubMed: 29551268]

Nakamura K, Imai Y, Nakamura A, and Yamane K (1992). Small cytoplasmic RNA of Bacillus subtilis: functional relationship with human signal recognition particle 7S RNA and Escherichia coli 4.5S RNA. J. Bacteriol. 174, 2185–2192. [PubMed: 1372600]

Netterling S, Bäreclev C, Vaitkevicius K, and Johansson J (2015). RNA Helicase Important for Listeria monocytogenes Hemolytic Activity and Virulence Factor Expression. Infect. Immun. 84, 67–76. [PubMed: 26483402]

Nielsen JS, Lei LK, Ebersbach T, Olsen AS, Klitgaard JK, Valentin-Hansen P, and Kallipolitis BH (2010). Defining a role for Hfq in Gram-positive bacteria: evidence for Hfq-dependent antisense regulation in Listeria monocytogenes. Nucleic Acids Res. 38, 907–919. [PubMed: 19942685]

Nielsen JS, Larsen MH, Lillebæk EM, Bergholz TM, Christiansen MH, Boor KJ, Wiedmann M, and Kallipolitis BH (2011). A small RNA controls expression of the chitinase ChiA in Listeria monocytogenes. PLoS ONE 6, e19019. [PubMed: 21533114]

Oliva G, Sahr T, and Buchrieser C (2015). Small RNAs, 5′ UTR elements and RNA-binding proteins in intracellular bacteria: impact on metabolism and virulence. FEMS Microbiol. Rev. 39, 331–349. [PubMed: 26009640]

Pain A, Ott A, Amine H, Rochat T, Bouloc P, and Gautheret D (2015). An assessment of bacterial small RNA target prediction programs. RNA Biol. 12, 509–513. [PubMed: 25760244]

Port GC, and Freitag NE (2007). Identification of novel Listeria monocytogenes secreted virulence factors following mutational activation of the central virulence regulator, PrfA. Infect. Immun. 75, 5886–5897. [PubMed: 17938228]

Quereda JJ, Ortega AD, Pucciarelli MG, and García-Del Portillo F. (2014). The Listeria Small RNA Rli27 Regulates a Cell Wall Protein inside Eukaryotic Cells by Targeting a Long 5′-UTR Variant. PLoS Genet. 10, e1004765. [PubMed: 25356775]

Raina M, King A, Bianco C, and Vanderpool CK (2018). Dual-Function RNAs. Microbiol. Spectr. 6, RWR-0032–2018.

Reniere ML, Whiteley AT, Hamilton KL, John SM, Lauer P, Brennan RG, and Portnoy DA (2015). Glutathione activates virulence gene expression of an intracellular pathogen. Nature 517, 170–173. [PubMed: 25567281]

Righetti F, Nuss AM, Twittenhoff C, Beele S, Urban K, Will S, Bernhart SH, Stadler PF, Dersch P, and Narberhaus F (2016). Temperature-responsive in vitro RNA structurome of Yersinia pseudotuberculosis. Proc. Natl. Acad. Sci. USA 113, 7237–7242. [PubMed: 27298343]

Ripio MT, Domínguez-Bernal G, Lara M, Suárez M, and Vazquez-Boland JA (1997). A Gly145Ser substitution in the transcriptional activator PrfA causes constitutive overexpression of virulence factors in Listeria monocytogenes. J. Bacteriol. 179, 1533–1540. [PubMed: 9045810]

Ross JA, Thorsing M, Lillebæk EMS, Teixeira Dos Santos P., and Kallipolitis BH (2019). The LhrC sRNAs control expression of T cell-stimulating antigen TcsA in Listeria monocytogenes by decreasing tcsA mRNA stability. RNA Biol. 16, 270–281. [PubMed: 30706751]

Ruiz de los Mozos I., Vergara-Irigaray M, Segura V, Villanueva M, Bitarte N, Saramago M, Domingues S, Arraiano CM, Fechter P, Romby P, et al. (2013). Base pairing interaction between 5′- and 3′-UTRs controls icaR mRNA translation in Staphylococcus aureus. PLoS Genet. 9, e1004001. [PubMed: 24367275]

Schmid B, Klumpp J, Raimann E, Loessner MJ, Stephan R, and Tasara T (2009). Role of cold shock proteins in growth of Listeria monocytogenes under cold and osmotic stress conditions. Appl. Environ. Microbiol. 75, 1621–1627. [PubMed: 19151183]

Sharma CM, Darfeuille F, Plantinga TH, and Vogel J (2007). A small RNA regulates multiple ABC transporter mRNAs by targeting C/A-rich elements inside and upstream of ribosome-binding sites. Genes Dev. 21, 2804–2817. [PubMed: 17974919]

Sievers S, Sternkopf Lillebæk EM, Jacobsen K, Lund A, Mollerup MS, Nielsen PK, and Kallipolitis BH (2014). A multicopy sRNA of Listeria monocytogenes regulates expression of the virulence adhesin LapB. Nucleic Acids Res. 42, 9383–9398. [PubMed: 25034691]

Sievers S, Lund A, Menendez-Gil P, Nielsen A, Storm Mollerup M, Lambert Nielsen S, Buch Larsson P., Borch-Jensen J, Johansson J, and Kallipolitis BH (2015). The multicopy sRNA LhrC controls expression of the oligopeptide-binding protein OppA in Listeria monocytogenes. RNA Biol. 12, 985–997. [PubMed: 26176322]

Strobel EJ, Yu AM, and Lucks JB (2018). High-throughput determination of RNA structures. Nat. Rev. Genet. 19, 615–634. [PubMed: 30054568]

Sun AN, Camilli A, and Portnoy DA (1990). Isolation of Listeria monocytogenes small-plaque mutants defective for intracellular growth and cell-to-cell spread. Infect. Immun. 58, 3770–3778. [PubMed: 2172168]

Thorvaldsdóttir H, Robinson JT, and Mesirov JP (2013). Integrative Genomics Viewer (IGV): high-performance genomics data visualization and exploration. Brief. Bioinform. 14, 178–192. [PubMed: 22517427]

Toledo-Arana A, Dussurget O, Nikitas G, Sesto N, Guet-Revillet H, Balestrino D, Loh E, Gripenland J, Tiensuu T, Vaitkevicius K, et al. (2009). The Listeria transcriptional landscape from saprophytism to virulence. Nature 459, 950–956. [PubMed: 19448609]

Updegrove TB, Zhang A, and Storz G (2016). Hfq: the flexible RNA matchmaker. Curr. Opin. Microbiol. 30, 133–138. [PubMed: 26907610]

Vogel J, and Sharma CM (2005). How to find small non-coding RNAs in bacteria. Biol. Chem. 386, 1219–1238. [PubMed: 16336117]

Waters LS, and Storz G (2009). Regulatory RNAs in bacteria. Cell 136, 615–628. [PubMed: 19239884]

Waters SA, McAteer SP, Kudla G, Pang I, Deshpande NP, Amos TG, Leong KW, Wilkins MR, Strugnell R, Gally DL, et al. (2017). Small RNA interactome of pathogenic E. coli revealed through crosslinking of RNase E. EMBO J. 36, 374–387. [PubMed: 27836995]

Wright PR, Georg J, Mann M, Sorescu DA, Richter AS, Lott S, Kleinkauf R, Hess WR, and Backofen R (2014). CopraRNA and IntaRNA: predicting small RNA targets, networks and interaction domains. Nucleic Acids Res. 42, W119–W123. [PubMed: 24838564]

Wu X, and Bartel DP (2017). Widespread influence of 3'fend structures on mammalian mRNA processing and stability. Cell 169, 905–917.e11. [PubMed: 28525757]

Wurtzel O, Sesto N, Mellin JR, Karunker I, Edelheit S, Bécavin C, Archambaud C, Cossart P, and Sorek R (2012). Comparative transcriptomics of pathogenic and non-pathogenic Listeria species. Mol. Syst. Biol. 8, 583. [PubMed: 22617957]

Zemansky J, Kline BC, Woodward JJ, Leber JH, Marquis H, and Portnoy DA (2009). Development of a mariner-based transposon and identification of Listeria monocytogenes determinants, including the peptidyl-prolyl isomerase PrsA2, that contribute to its hemolytic phenotype. J. Bacteriol. 191, 3950–3964. [PubMed: 19376879]

Zhang Y, Burkhardt DH, Rouskin S, Li GW, Weissman JS, and Gross CA (2018). A Stress Response that Monitors and Regulates mRNA Structure Is Central to Cold Shock Adaptation. Mol. Cell 70, 274–286.e7. [PubMed: 29628307]

Zubradt M, Gupta P, Persad S, Lambowitz AM, Weissman JS, and Rouskin S (2017). DMS-MaPseq for genome-wide or targeted RNA structure probing in vivo. Nat. Methods 14, 75–82. [PubMed: 27819661]

Highlights

- FUSE can identify and structurally characterize regulatory events in 5′ UTRs
- An mRNA encoding listeriolysin O stabilizes the mRNA encoding its chaperone PrsA2
- An RNA thermoswitch controls expression of the CspA protein in *L. monocytogenes*
- Simultaneous binding of ribosomes and small RNAs on an mRNA can be defined by FUSE

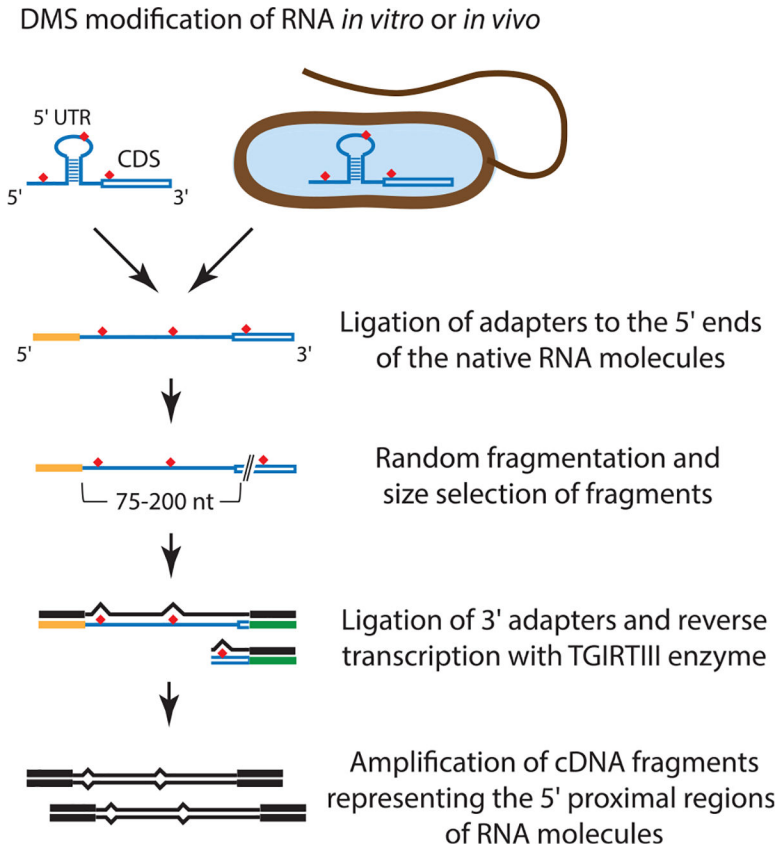

Figure 1. The Strategy for Preparation of FUSE Libraries

Bacterial cells were treated with DMS. Alternatively, RNA isolated from cells was refolded, and DMS modification was performed in *vitro*. Ligation of RNA adapters to the 5′ ends of the native RNA molecules allowed selective amplification of cDNA fragments representing the 5′ proximal regions of mRNAs and the whole length of most small RNAs (sRNAs). See also Figure S1 and Tables S1 and S2.

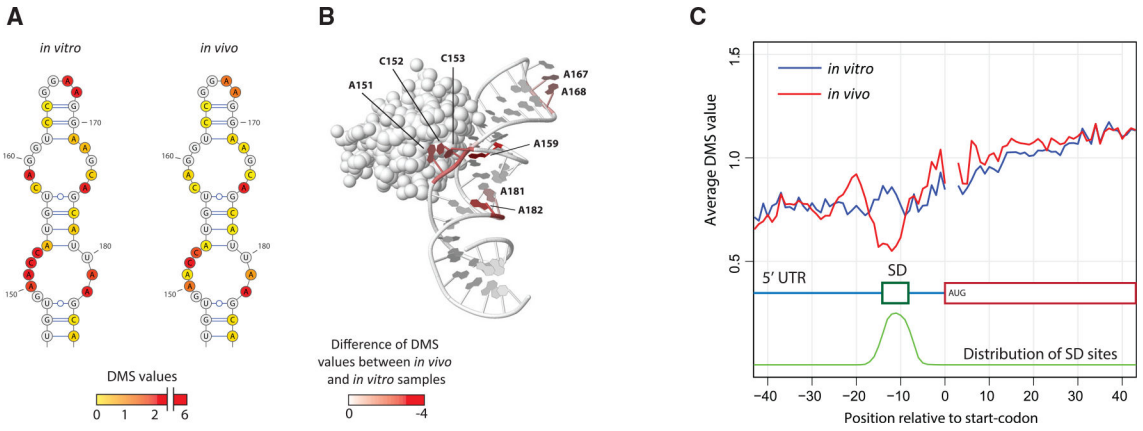

Figure 2. DMS Protection *In Vivo* Can Be Caused by Interaction with Proteins or Ribosomes

(A) DMS values of nucleotides in domain IV of the structurally conserved 4.5S RNA *in vivo* and *in vitro*. The structure of 4.5S RNA in *L. monocytogenes* was modeled on the basis of homology with 4.5S RNA in *E. coli*. Red color denotes high DMS values of adenine "A" and cytosine "C" nucleotides indicating their unpaired status. On the contrary, yellow color indicates low DMS values, suggesting the nucleotides to be base paired or interacting with a protein.

(B) The nucleotides of domain IV of 4.5S RNA showing decreased DMS values *in vivo* are located at the site of interaction with the Ffh protein. The crystal structure represents the M domain of the Ffh protein interacting with domain IV of 4.5S RNA in *E. coli*. (PDB: 1HQ1) (Batey et al., 2001). The evolutionarily conserved nucleotides are colored according to the differences of DMS values between *in vivo* and *in vitro* samples. Intensive red color indicates nucleotides with strongly decreased DMS values *in vivo*.

(C) The SD sequences are protected by ribosomes *in vivo*. The average DMS values in the vicinity of the start codon are shown *in vitro* (blue line) and *in vivo* (red line). Because the start codons always have a U at the second and a G at the third position, DMS values cannot be calculated for these positions. The distribution of SD sequence locations is plotted as a green line.

See also Figure S2 and Table S3.

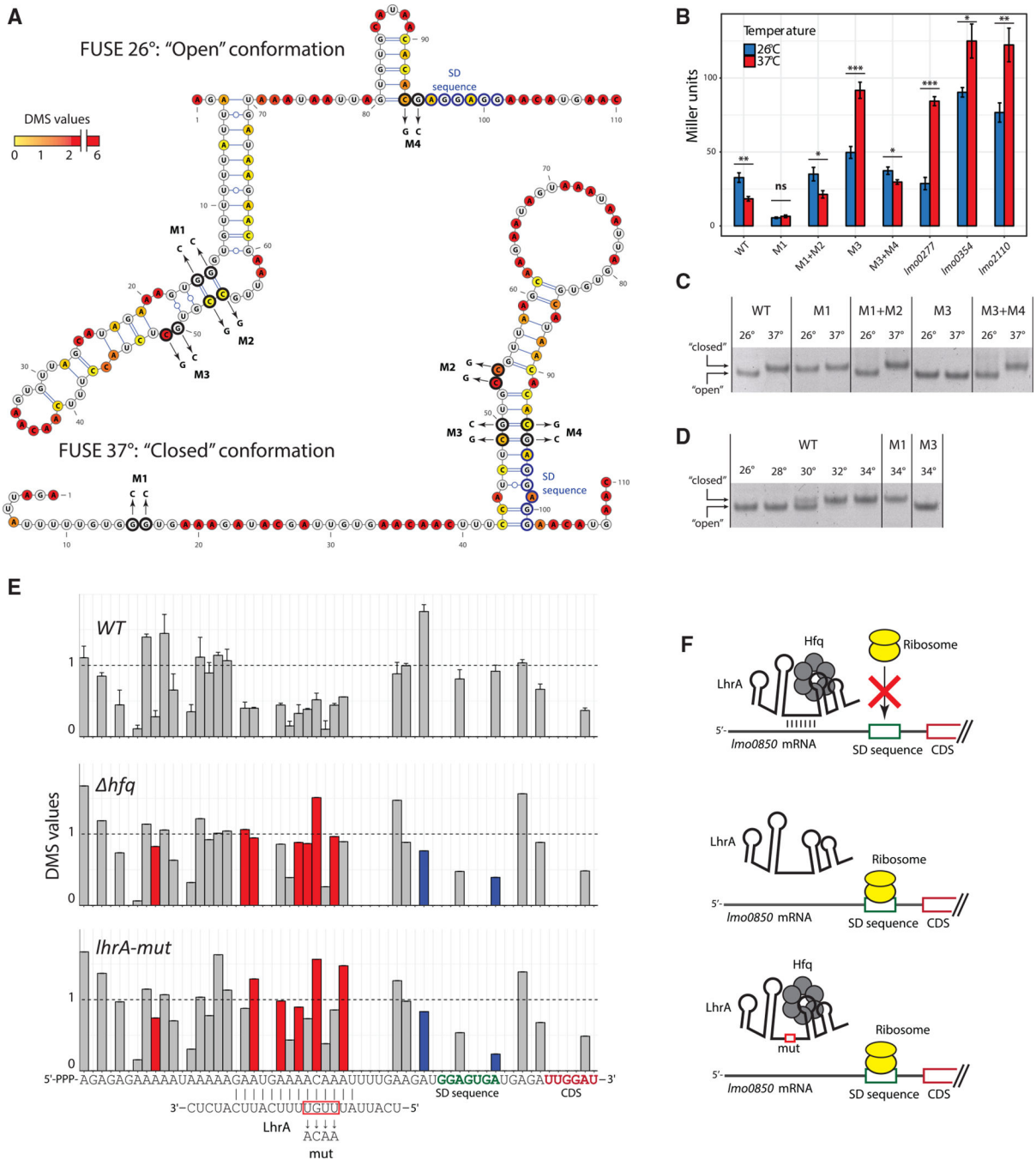

Figure 3. FUSE Identifies an RNA Thermosensor and Determines Simultaneous Binding of an sRNA and the Ribosome to an mRNA

(A) The 5′ UTR of *cspA* (*lmo1364*) mRNA assumes alternative conformations at different temperatures. The secondary structures of the "open" and "closed" conformations are shown with DMS values of the 26°C sample for the open conformation and the 37°C sample for the closed conformation. A red color denotes high DMS values of adenine (A) and cytosine (C) nucleotides indicating their unpaired status. On the contrary, a yellow color indicates low DMS values suggesting the nucleotides to be base paired or interacting with a protein. The locations of mutations M1–M4 are indicated.

(B) The *cspA* 5′ UTR inhibits translation at 37°C, and this effect is mediated by the rearrangement of its structure. The coding sequence of the β-galactosidase gene was fused with the *cspA* 5′ UTR (wild type [WT]), the *cspA* 5′ UTR carrying mutations M1–M4 (see A for their location) and the 5′ UTRs of control mRNAs (*lmo0277*, *lmo0354*, and *lmo2110*, respectively). The constructs were expressed in *E. coli* at different temperatures, and β-galactosidase activity was measured (n = 3). The error bars represent standard deviations. The statistically significant differences between β-galactosidase expression levels at 26°C and 37°C are shown by asterisks (Student's t test, *p < 0.05; **p < 0.01; ***p < 0.001).
(C) Electrophoretic mobility of *in-vitro*-synthesized WT and mutant *cspA* 5′ UTRs at 26°C and 37°C. The location of the mutations M1–M4 are shown in (A). The *in-vitro*-transcribed *cspA* 5′ UTR and the mutants were denatured, refolded at the indicated temperatures, and resolved on non-denaturing polyacrylamide gel. The experiments were repeated twice with similar results. Pictures were 1.5 times extended on the vertical axis to facilitate visualization.
(D) The rearrangement of the *cspA* 5′ UTR structure *in vitro* upon the temperature increase. The *in-vitro*-transcribed *cspA* 5′ UTR was denatured and refolded at 26°C. Gradual increase in temperature induced structural rearrangement at approximately 30°C. M1 and M3 mutants locked in the "closed" and "open" conformations, respectively, are shown as controls.
(E) DMS values of the *lmo0850* 5′ UTR in the WT, *Δhfq*, and *lhrA-mut* strains, respectively. Red bars indicate statistically significant increase of DMS values, and blue bars indicate statistically significant decrease of DMS values in the *Δhfq* and the *lhrA-mut* strains relative to the WT strain, respectively. The error bars for the WT strain represent standard deviation (n = 2).
(F) Model of the interaction between *lmo0850* mRNA, LhrA sRNA, Hfq protein, and the ribosome. Binding of LhrA inhibits ribosome binding to the SD sequence of *lmo0850*. Absence of Hfq or a mutation in LhrA (at its interaction site with *lmo0850*) decreases LhrA binding to *lmo0850* and thus increases ribosome binding to the SD region.
See also Figures S3 and S4 and Table S4.

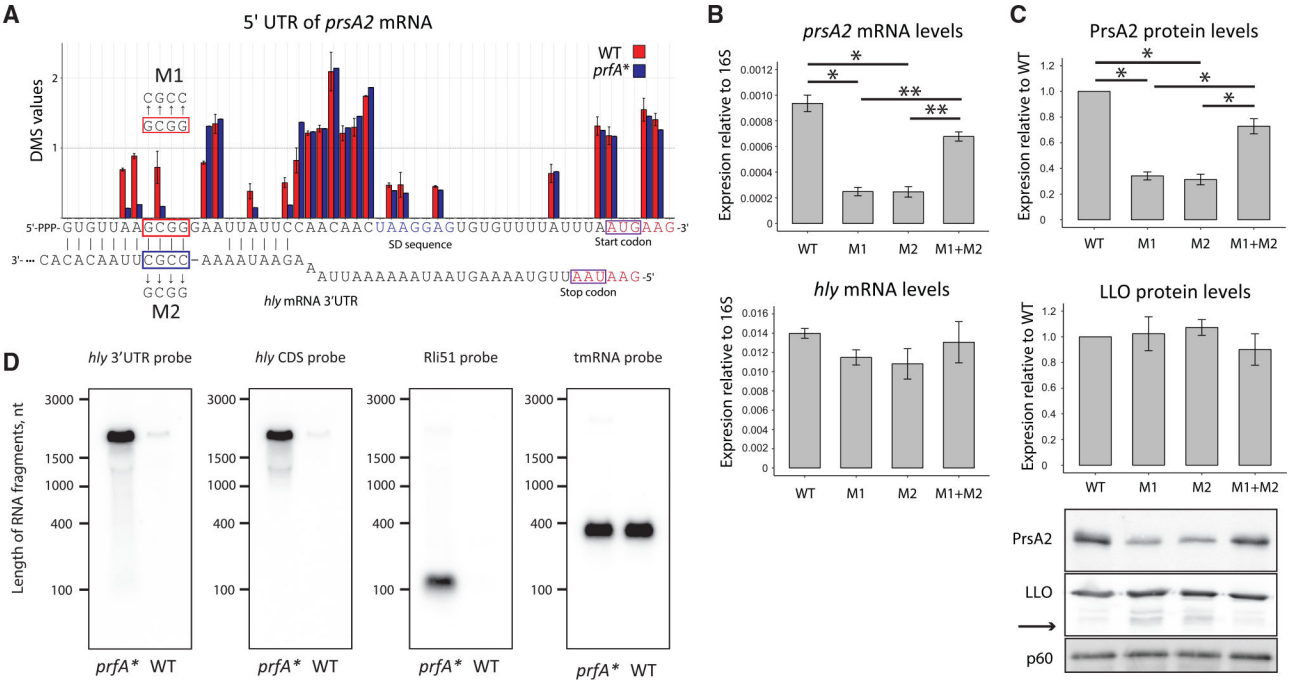

Figure 4. The 3′ UTR of Full-Length *hly* mRNA Interacts with the 5′ UTR of *prsA2* mRNA, thereby Increasing the Level of *prsA2* mRNA and PrsA2 Protein

(A) Several nucleotides in the 5′ UTR of *prsA2* mRNA show reduced DMS values in a *prfA** strain relative to the WT strain. The stretch of DMS-protected nucleotides corresponds to the predicted base-pairing interaction with the 3′ UTR of *hly* mRNA. Red and blue boxes indicate the locations of the M1 and M2 mutations, respectively. Inset shows sequence of the M1 and M2 mutations, respectively. The start codon of *prsA2* and the stop codon of *hly* are indicated by purple boxes. The error bars for the WT strain represent standard deviation (n = 2).

(B) Expression of *prsA2* and *hly* genes in the WT strain and strains carrying mutations M1, M2, and M1+M2, respectively. Expression of the genes was measured by qRT-PCR, and the data were normalized to the expression level of 16S rRNA (n = 3). The error bars represent standard deviation, and the statistically significant differences in the levels of mRNAs are shown by asterisks (Student's t test, *p < 0.05, **p < 0.01).

(C) Expression of PrsA2, LLO, and P60 (control) in the WT strain and strains carrying mutations M1, M2, and M1+M2, respectively. Expression of the proteins was measured by western blot, and the data were normalized to the expression level in the WT strain. Representative western blots showing PrsA2, LLO, and P60 levels are shown (n = 2). The error bars represent standard deviation, and the statistically significant differences in the levels of proteins are shown by asterisks (Student's t test, *p < 0.05). The products of partial proteolysis or truncated LLO proteins in M1 and M2 strains are indicated by an arrow.

(D) The 3′ UTR of *hly* mRNA binding to *prsA2* is part of the full-length *hly* transcript. Northern blot was performed with RNA isolated from the *prfA** and the WT strains. The membrane was probed with radioactively labeled oligonucleotides complementary to the 3′ UTR (*hly* 3′ UTR probe) and the coding sequence (*hly* CDS probe) of *hly* mRNA. To demonstrate the ability to detect short transcripts, the membrane was probed with

oligonucleotides complementary to the PrfA-regulated sRNA Rli51, originating from the 5′ UTR of *mpl*. The probe complementary to the transfer-messenger RNA (tmRNA) was used as a loading control.

See also Figure S5 and Table S5.

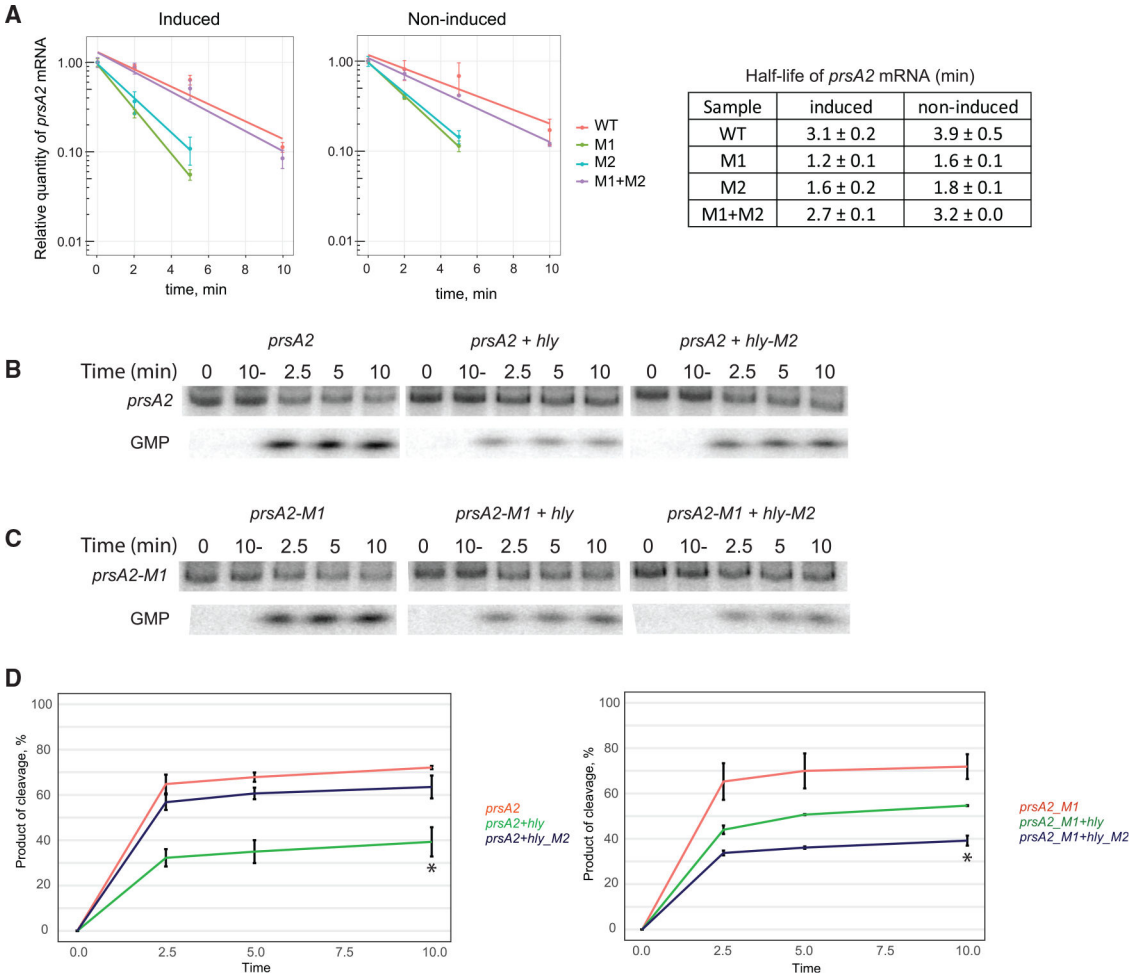

Figure 5. Interaction with *hly* Protects *prsA2* mRNA from Degradation by RNase J1

(A) The half-life of *prsA2* mRNA in *L. monocytogenes* EGDe (WT) strain and *prsA2* and *hly* UTR mutants under inducing and non-inducing conditions. RNA was isolated from indicated strains grown at virulence-inducing or non-inducing conditions, respectively, at indicated time points after addition of rifampicin. The *prsA2* transcript was detected by northern blot (representative figure is shown in Figure S5D) and quantified before being normalized to the quantity of tmRNA. The expression levels were normalized to the expression level before rifampicin addition (0 min) for each strain, respectively. For each time point, the mean and standard deviation of two measurements are shown. For each sample, the fitted log-linear curve that was used for half-life calculations is shown. In the WT and M1+M2 samples, the 0-, 2-, 5-, and 10-min time points after rifampicin addition were used for half-life calculations. For the M1 and M2 samples, the 0-, 2-, and 5-min time points after rifampicin addition were used for half-life calculations. Because *prsA2* had very low quantities at 10 min in these strains, this time point was excluded from half-life calculations. The data in the table (right) represent the mean and 95% confidence interval calculated on the basis of two measurements.

(B) The 3′ UTR of *hly* mRNA protects the 5′ UTR of *prsA2* mRNA from degradation by RNase J1 *in vitro*. The RNA fragments corresponding to the first 53 nt of the *prsA2* mRNA

carrying a ^{32}P-labeled 5′-monophosphate group. The fragment was incubated with RNase J1 for the indicated amount of time in the absence or in the presence of WT *hly* transcript (*hly*) ora *hly* transcript carrying the M2 mutations (*hly-M2*). In parallel, the control was incubated in the absence of the enzyme (10−). The bands correspond to the full-length *prsA2* 5′ UTR and its fragments (upper panels) and the released GMP (lower panels).

(C) The 3′ UTR of *hly-M2* mRNA protects the 5′ UTR of *prsA2-M1* from degradation by RNase J1 *in vitro*. The RNA fragments corresponding to the first 53 nt of *prsA2-M1* mRNA carrying a ^{32}P-labeled 5′-monophosphate group. The fragment was incubated with RNase J1 for the indicated amount of time in the absence or in the presence of WT *hly* transcript (*hly*) or a *hly* transcript carrying the M2 mutations (*hly-M2*). In parallel, the control was incubated in the absence of the enzyme (10-). The bands correspond to the full-length *prsA2* and fragments (upper panels) and the released GMP (lower panels).

(D) The dynamics of GMP release from *prsA2* (left panel) and *prsA2-M1* (right panel) substrate RNAs by RNase J1 ± *hly* or *hly-M2* mRNAs. The data shown correspond to the quantification of two independent experiments from Figures 5B and 5C (technical replicates). The error bars represent standard deviations, and the asterisks indicate statistically significant differences in the amounts of released GMP after 10-min incubation for *prsA2* versus *prsA2+hly* and *prsA2-M1* versus *prsA2-M1+hly-M2* (Student's t test, *p < 0.05).

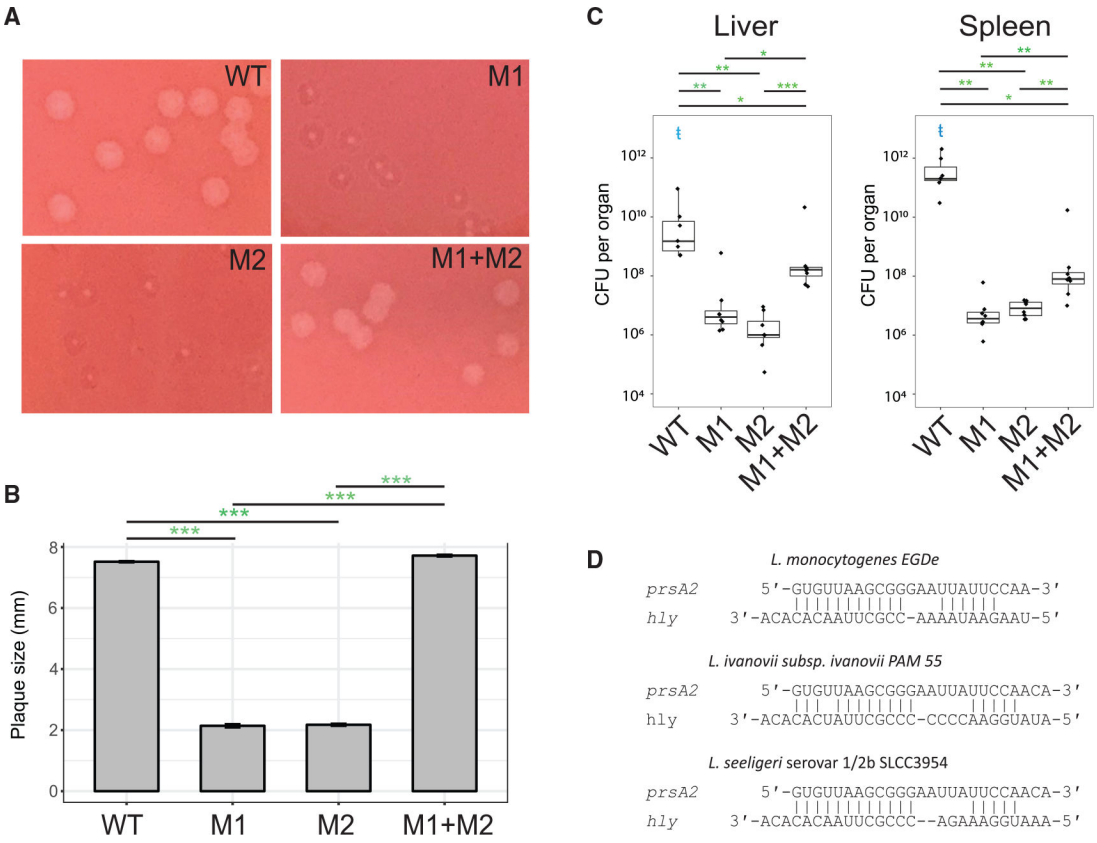

Figure 6. The *hly-prsA2* Interaction Is Important for *L. monocytogenes* Infection and Is Conserved in All Hemolytic *Listeria* Species

(A) Intracellular growth and cell-to-cell spread of bacterial strains. A representative plaque assay is shown where monolayers of mouse L2 fibroblasts were infected with the indicated *Listeria monocytogenes* strains and plaque formation was determined in the presence of gentamicin 72 h post-infection. 20 plaques were measured in three independent experiments for all strains.

(B) Measurements represent plaque size formed by the indicated strains with respect to the WT strain in millimeters (mm). Error bars represent the standard error of the mean. The statistically significant differences between plaque size are shown by asterisks (green) (Student's t test, ***p < 0.001).

(C) The abolishment of the interaction between *prsA2* and *hly* mRNAs attenuates *L. monocytogenes* virulence. Mice were infected by tail vein injection with 2×10^4 colony-forming units (CFUs) of the indicated strain. At 72 h post-infection, livers and spleens were harvested, homogenized, and plated for bacterial burdens. Boxplots are shown where each dot represents one mouse. Data were obtained from eight animals. An asterisk (green) indicates statistical significance estimated by two-tailed Wilcoxon rank-sum test when M1 and M2 strains were compared with WT or M1+M2 strains (*p < 0.05, **p < 0.01, ***p < 0.001). ŧ (light blue) indicates that one mouse succumbed to infection prior to 72 h for WT strain.

(D) The interaction site between *prsA2* and *hly* mRNAs is conserved in all *Listeria* species carrying the *hly* gene (*L. monocytogenes*, *L. ivanovii*, and *L. seeligeri*, respectively).

See also Figure S6.

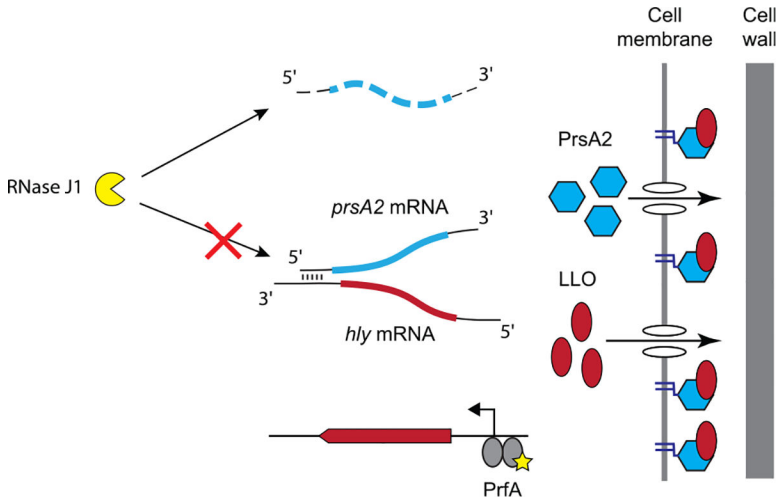

Figure 7. Interaction between mRNAs Couples Expression Level of the PrsA2 Chaperone with Its Substrate Listeriolysin O

In the absence of the mRNA-mRNA interaction, the *prsA2* transcript (blue line) is degraded by the exoribonuclease RNase J1 (yellow). When the major virulence regulator PrfA becomes activated (gray ovals with yellow star), transcription of the *hly* mRNA encoding the secreted virulence factor listeriolysin O (LLO; red oval) is induced. The 3′ UTR of the *hly* mRNA base pairs with the extreme 5′ end of the *prsA2* mRNA and protects it from RNase J1-mediated degradation. Outside the cell membrane, PrsA2 chaperone (blue hexagon) activity facilitates the proper folding of LLO and other virulence factors.

KEY RESOURCES TABLE

REAGENT or RESOURCE	SOURCE	IDENTIFIER
Antibodies		
Anti-Listeriolysin (LLO) antibody	Abcam	Cat# ab200538
Anti-P60 antibody	Biosite	Cat# P6017
Rabbit polyclonal anti-PrsA2 antibody	(Alonzo et al., 2009)	N/A
Polyclonal anti-ActA antibody	(Netterling et al., 2015)	N/A
Anti-rabbit-horseradish peroxidase secondary antibody	Agrisera	Cat# AS09 602
Bacterial and Virus Strains		
Listeria monocytogenes EGD-e	(MacKaness, 1964)	N/A
L. monocytogenes EGD-e Δhfq	(Christiansen et al., 2004)	N/A
L. monocytogenes EGD-e LhrA_mut	(Nielsen et al., 2010)	N/A
L. monocytogenes EGD-e prfA*	(Goodetal., 2016)	N/A
L. monocytogenes EGD-e 5UTR2219-M1	This study	N/A
L. monocytogenes EGD-e 3UTR0202-M2	This study	N/A
L. monocytogenes EGD-e 5UTR2219-M1 3UTR0202-M2	This study	N/A
L. monocytogenes EGD-e prfA* 5UTR2219-M1	This study	N/A
L. monocytogenes EGD-e prfA* 3UTR0202-M2	This study	N/A
Chemicals, Peptides, and Recombinant Proteins		
Purified C-terminal His tagged RNase J1	(Mathy et al., 2007)	N/A
Deposited Data		
Raw and analyzed NGS data	This study	GEO: GSE118387
Scripts for data analysis	This study	https://github.com/dimaignatov/5-UTR-structure-elucidation
Experimental Models: Cell Lines		
L2 mouse fibroblasts	(Sun et al., 1990)	N/A
Experimental Models: Organisms/Strains		
Swiss Webster (CFW) Mouse, female	Charles River Laboratories	Cat# 024, https://www.criver.com/products-services/find-model/swiss-webster-cfw-mouse?region=3616
Oligonucleotides		
See Table S6		N/A
Recombinant DNA		
See Table S8		N/A

REAGENT or RESOURCE	SOURCE	IDENTIFIER
Software and Algorithms		
Bowtie2	Langmead and Salzberg, 2012	http://bowtie-bio.sourceforge.net/bowtie2/index.shtml
HTSeq framework	Anders et al., 2015	https://htseq.readthedocs.io/en/release_0.11.Vindex.html
Integrative Genomics Viewer	Thorvaldsdottir et al., 2013	https://software.broadinstitute.org/software/igv/
VARNA	Darty et al., 2009	http://varna.lri.fr/
RNAfold WebServer	Lorenz et al., 2011	http://rna.tbi.univie.ac.at//cgi-bin/RNAWebSuite/RNAfold.cgi
T-Coffee Multiple Sequence Alignment Server	Di Tommaso et al., 2011	http://tcoffee.crg.cat/